



**A**t its core, reticular chemistry has translated the precision and expertise of organic and inorganic synthesis to the solid state. While initial excitement over metal–organic frameworks (MOFs) and covalent organic frameworks (COFs) was undoubtedly fueled by their unprecedented porosity and surface areas, the most profound scientific innovation of the field has been the elaboration of design strategies for the synthesis of extended crystalline solids through strong directional bonds. In this contribution we highlight the different classes of reticular materials that have been developed, how these frameworks can be functionalized, and how complexity can be introduced into their backbones. Finally, we show how the structural control over these materials is being extended from the molecular scale to their crystal morphology and shape on the nanoscale, all the way to their shaping on the bulk scale.

## 1. Introduction

Reticular chemistry (based on the Latin *reticulum*: small net) as exemplified by metal–organic frameworks (MOFs) and covalent organic frameworks (COFs) is concerned with linking molecular building blocks through strong bonds to form porous crystalline 2D and 3D frameworks in a designed manner.<sup>[1]</sup> 25 years ago, at the inception of the field, there was a noticeable absence of such structures which was generally ascribed to the challenge of crystallizing porous frameworks through strong directional bonds. This was in no small part due to a major disconnect between solid-state organic and inorganic synthesis at that time. Fundamentally, organic synthesis makes use of covalent bond formation, thus

## From the Contents

<b>1. Introduction</b>	23947
<b>2. Synthesis of MOFs</b>	23949
<b>3. Multicomponent MOFs</b>	23951
<b>4. Multivariate MOFs</b>	23952
<b>5. Synthesis of COFs</b>	23953
<b>6. Synthesis of ZIFs</b>	23956
<b>7. Characterization of Reticular Materials</b>	23957
<b>8. Computational Modelling of Reticular Frameworks</b>	23958
<b>9. Postsynthetic Modification</b>	23960
<b>10. MOF Nanoparticles</b>	23962
<b>11. Reticular Thin Films</b>	23964
<b>12. MOFs at the Mesoscopic and Macroscopic Scale</b>	23965
<b>13. Outlook</b>	23968

[\*] R. Freund

Solid State Chemistry, University of Augsburg  
86159 Augsburg (Germany)

Dr. S. Canossa  
EMAT, University of Antwerp  
2020 Antwerp (Belgium)

Prof. S. M. Cohen  
Department of Chemistry and Biochemistry  
University of California, San Diego (USA)

Dr. W. Yan, Prof. H. Deng  
College of Chemistry and Molecular Sciences  
Wuhan University, Wuhan (China)

Dr. V. Guillermin, Prof. M. Eddaoudi  
Functional Materials Design, Discovery and Development Research  
Group (FMD3)

Advanced Membranes and Porous Materials Center  
Division of Physical Sciences and Engineering, King Abdullah  
University of Science and Technology (KAUST)  
Thuwal 23955-6900 (Saudi Arabia)

Dr. D. G. Madden, Prof. D. Fairen-Jimenez  
Adsorption & Advanced Materials Laboratory (A<sup>2</sup>ML)  
Department of Chemical Engineering & Biotechnology  
University of Cambridge (UK)

H. Lyu, O. Zaremba  
Department of Chemistry, University of California, Berkeley (USA)

Dr. L. K. Macreadie  
School of Chemistry, University of Sydney (Australia)

Dr. Z. Ji

Department of Chemistry, Stanford University (USA)

Dr. Y. Zhang, Prof. B. Wang  
Advanced Research Institute of Multidisciplinary Science  
School of Chemistry and Chemical Engineering  
Beijing Institute of Technology  
Beijing (China)

Dr. F. Haase, Prof. Dr. C. Wöll  
Institute of Functional Interfaces (IFG)  
Karlsruhe Institute of Technology (KIT)  
Eggenstein-Leopoldshafen (Germany)

O. Zaremba, Dr. J. Andreo, Prof. Dr. S. Wuttke  
BCMaterials, Basque Center for Materials  
UPV/EHU Science Park, Leioa 48940 (Spain)  
E-mail: stefan.wuttke@bcmaterials.net

Prof. Dr. S. Wuttke  
IKERBASQUE, Basque Foundation for Science  
Bilbao (Spain)

Dr. C. S. Diercks  
Department of Chemistry, The Scripps Research Institute  
La Jolla, California 92037 (USA)  
E-mail: cdiercks@scripps.edu

 The ORCID identification number(s) for the author(s) of this article can be found under:  
<https://doi.org/10.1002/anie.202101644>.

enabling the rational multistep synthesis of complex natural products and polymers. However, the lack of microscopic reversibility of such reactions complicates the crystallization into extended 2D and 3D lattices through strong bonds, and prior to the development of reticular chemistry, rational organic synthesis was limited to discrete molecular and 1D polymeric structures. In contrast, inorganic synthesis is often carried out under thermodynamic control, which allows for the synthesis of highly symmetric discrete and extended architectures from simple precursors in a single step. The thermodynamic control over product formation does, however, complicate the rational design of the size and shape of molecular species and, in the case of extended structures, favors the formation of dense crystals. This difference can best be highlighted by the syntheses of the complex organic natural product taxol, a multistep synthesis with overall low yield, and that of the inorganic ferrous wheel, a highly symmetric and near-quantitative one-step assembly from simple precursors.

The synthesis of the first MOFs, MOF-2 and MOF-5, addressed this challenge by reticulating inorganic polynuclear secondary building units, fragments of metal oxides, with shape-persistent organic linkers through strong bonds.<sup>[2,3]</sup> Here, the bond formation of the constituent inorganic secondary building units (SBUs) enabled crystallization, while the shape-persistent organic terephthalate linkers opened up the structure and endowed the frameworks with permanent porosity. In contrast to early reported coordination polymers and discrete coordination architectures,<sup>[4-6]</sup> the organic and inorganic units in MOFs are linked through strong (charged metal-carboxylate) and directional (bridging carboxylate binding mode) bonds. This was essential to the development of the field, as it led to permanently porous frameworks with surface areas exceeding that of all other materials known to date.<sup>[7,8]</sup> The marriage of covalent organic and inorganic chemistry in reticular frameworks has enabled unprecedented control over the design of porous materials, and the vast possibilities of linking the many amenable inorganic clusters and organic linkers has rendered these materials the most diverse class of extended crystals today (> 100 000 different structures).<sup>[9-13]</sup>

The development of COFs, a second class of reticular frameworks comprised entirely of molecular organic building units linked through covalent bonds, required the elaboration

of synthesis conditions that allow for the microscopic reversibility of covalent bond formation to enable crystallization.<sup>[14]</sup> This was achieved for the first time in 2005 for 2D (COF-1 and COF-5)<sup>[15]</sup> and in 2007 for 3D structures (COF-105 and COF-108).<sup>[16]</sup> The fact that reticulation was achieved through highly directional covalent boroxine and boronate ester bonds between shape-persistent organic molecules not only endowed these COFs with high internal surface areas but also made the a priori design of their structure type and metrics highly accurate. Since this initial report, reticulation reactions in COFs have been extended to a myriad of organic transformations, and today COFs extend the retrosynthetic principle of organic synthesis from molecules and 1D polymers to 2D and 3D organic extended structures.

Reticular chemistry begins with the identification of a target structure, which is deconstructed into its fundamental geometric units to determine the underlying topology and identify the molecular constituents that represent the shape and connectivity of these units. This approach dates back to early works on the geometrical description of crystal chemistry.<sup>[17,18]</sup> Reticulation, the assembly of these units through strong bonds into a robust crystalline lattice, yields the target structure. Optimization of the structure metrics can be achieved according to the isorecticular principle and functionality can be introduced through postsynthetic modification. Synthetic control in reticular chemistry further extends to control over the nanoscale (nanocrystals or films), to their structuring into mesoscopic objects and implementation into monoliths (Figure 1).<sup>[1,14,19]</sup>

From the very outset, reticular chemistry has been a highly multidisciplinary field that requires the expertise and know-how of scientists from various backgrounds, and the field has always defied what many previously considered “legitimate” divisions within the different subdisciplines of organic and inorganic chemistry, materials chemistry, and engineering. Today, scientists from diverse backgrounds work in the field and their unique contributions are at the very core of the continued progress in this area of research. In this Review, we aim to summarize the key milestones in the chemistry of reticular frameworks achieved by experts in the respective areas to give an all-encompassing overview of the state of the art in the field 25 years after its inception.



*Stefan Wuttke created the research group “WuttkeGroup for Science”, initially hosted at the Institute of Physical Chemistry at the University of Munich (LMU, Germany). Currently, he is an Ikerbasque Professor at the Basque Center for Materials, Applications and Nanostructures (BCMaterials, Spain). His research is focused on developing methodologies to write and read chemical information onto and from the backbone of hybrid framework materials. Further research interests include acquiring a fundamental understanding of the chemical and physical processes involved in their synthesis and functionalization.*



*Christian Diercks studied chemistry at the University of Heidelberg and carried out undergraduate research in the group of Prof. Jean-Pierre Sauvage at the University of Strasbourg (France), as well as at Northwestern University (USA) under the guidance of Sir James Fraser Stoddart. He obtained his Ph.D. from UC Berkeley under the mentorship of Prof. Omar M. Yaghi in 2018 for his work on covalent organic frameworks. Currently, he is a postdoctoral researcher in the group of Prof. Peter G. Schultz at the Scripps Research Institute, working on adding new chemistries to the processes of the central dogma of molecular biology.*

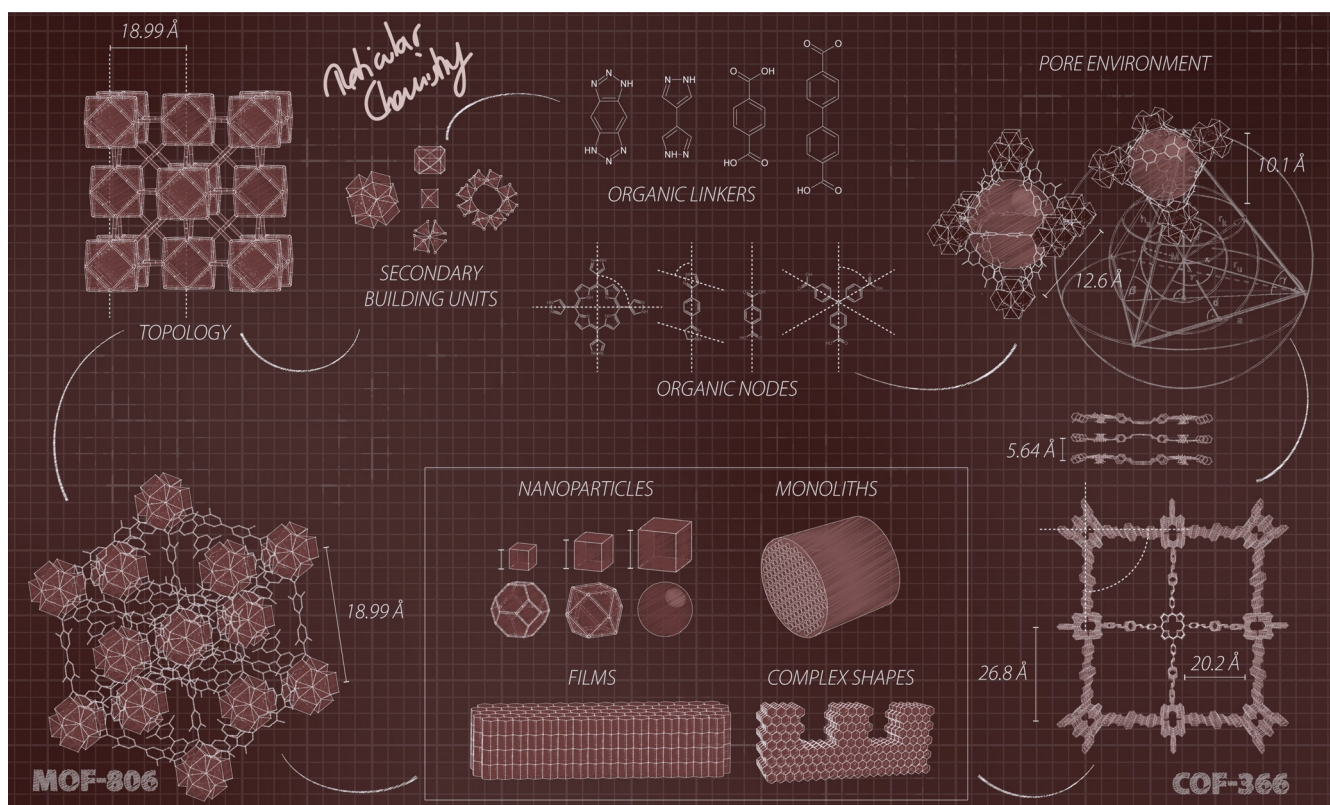


Figure 1. Design concepts in reticular chemistry.

## 2. Synthesis of MOFs

Coordination chemistry has long been explored for the synthesis of extended solids (coordination networks),<sup>[4]</sup> and for many years, consisted mainly of single metal ions linked by polytopic monodentate ligands such as bipyridines.<sup>[20]</sup> The flexibility around the angles of coordination metals and their diversity in coordination number allowed for the formation of various nets, suggesting the potential to construct a myriad of periodic structures with diverse underlying topologies. However, the encountered flexibility in single-metal-ion-based networks hindered their rational design due to a lack of control of the coordination bonds' directionality. Additionally, while relatively easily synthesized, these frameworks based on comparatively weak bonds were prompt to collapse upon evacuation of their pore content.

Therefore, two main parameters were needed for establishing permanent microporosity in these materials: 1) rigidity and directionality of the framework's constituents and 2) an increased bond strength between them. The development of rigid and directional molecular building blocks (MBBs) based on stronger metal–ligand binding was found to meet these requirements. It should be noted that phosphonates<sup>[21,22]</sup> and sulfonates<sup>[21]</sup> afforded the formation of highly stable frameworks, but their use in reticular chemistry remained limited. Explicitly, they do not provide the same level of predictable directionality as the ligand class that led to remarkable milestones in the design and synthesis of MOFs—carboxylates.<sup>[2,3,23–25]</sup>

### 2.1. Carboxylate-Based MOFs: The Breakthrough

The development of carboxylate-based MOFs marked a breakthrough in the field of porous materials, with key milestones that established MOFs as candidates for various key applications requiring porosity (Figure 2).

For instance, the selective adsorption of aromatic vs. aliphatic solvents was displayed by a 2-periodic Co-trimesate, thanks to preferred  $\pi$ – $\pi$  interactions.<sup>[23]</sup> Moreover, these MOFs showed permanent porosity when they were completely evacuated: the first fully reversible nitrogen adsorption isotherm for MOFs was recorded with 2-periodic **sql**-MOF (MOF-2).<sup>[2]</sup> It should be noted that gas adsorption measurements conducted either at constant pressure (isobar)<sup>[24]</sup> or at high pressures<sup>[26]</sup> were not considered at that time as definitive proof of the permanent porosity of MOFs, as they differed from the standard characterization used for conventional porous materials such as zeolites.

Further developments led to the discovery of HKUST-1<sup>[25]</sup> (Cu-trimesate with **tbo** topology) and MOF-5<sup>[3]</sup> (Zn-terephthalate with **pcu** topology). Both set porosity records at the time of their publication, but their influence went beyond just numbers, as they established themselves as the most prototypical and utilized MOFs in reticular chemistry for years. Importantly, the evolution of crystallization methods from slow diffusion in solvent or gels, to layering, to solvothermal methods facilitated the development of the field and allowed for higher yields.<sup>[25,27]</sup> Overall, establishing proper conditions for the formation of specific inorganic MBBs made it possible to explore the myriad ways with which they can be assembled

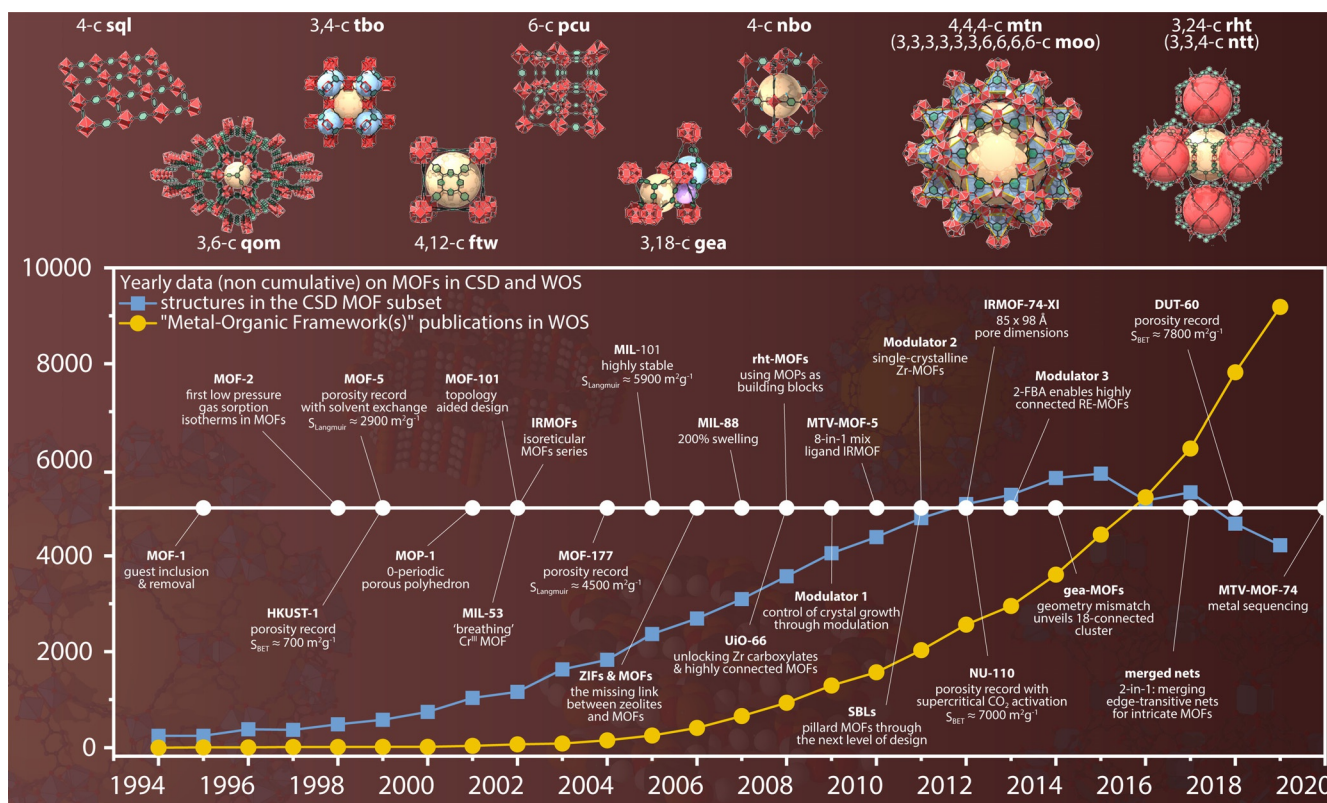


**Figure 2.** Top: A few carboxylate-based MOFs, reflecting chemical, structural, and topological diversity. Bottom: Timeline showing some major MOFs achievements, along with the yearly number of publications on MOFs and the number of MOF structures reported to the CSD.

together with organic ligands into 0-, 1-, 2-, or 3-periodic nets.<sup>[1]</sup>

## 2.2. Isoreticular MOFs

Once the appropriate reaction conditions providing a suitable chemical environment for the formation of a given MBB were identified, it became possible to rationally approach the design and assembly of isoreticular MOFs, using elongated or decorated ligands. The pioneering series of IRMOFs,<sup>[28]</sup> derived from MOF-5 with **pcu** topology,<sup>[3]</sup> initiated the development of isoreticular MOF platforms (i.e., MOFs sharing the same topology), while enabling the fine-tuning of their properties. Throughout the years, the strategy of isoreticular chemistry has been applied to a plethora of additional MOF platforms, such as **fcu**,<sup>[29]</sup> **rht/ntt**,<sup>[30–32]</sup> **nbo/fof**,<sup>[32,33]</sup> **acs**,<sup>[34,35]</sup> and **tbo**.<sup>[36,37]</sup> Along the way, major milestones have been reached, such as new porosity records (NU-110, DUT-60)<sup>[31,38]</sup> and ultralarge channels (85 × 98 Å in IRMOF-74-XI).<sup>[39]</sup>

## 2.3. The Touch of Rational Design

In parallel to the fruitful systematic screening of combinations of organic ligands with various metals, it was evident that a higher level of prediction in the assembly of MOFs was needed. This is where topology and geometrical consider-

ations found their major role. Aside from being an invaluable tool for the description and understanding of MOF structures,<sup>[40–42]</sup> topology, and particularly edge-transitive nets,<sup>[43]</sup> are a valuable asset owing to their design and identification of required geometrical attributes to achieve a given net. The first example of this strategy is the synthesis of MOF-101, where the steric hindrance generated by the bromo functionalization of a terephthalic acid forces the adjacent carboxylate to rotate out of plane.<sup>[44]</sup>

This approach has been developed throughout the years with the use of tilted,<sup>[45]</sup> bent,<sup>[45]</sup> and zigzag<sup>[46]</sup> ligands that generate a geometry mismatch and help in deviating from default topologies.<sup>[47]</sup> Once meticulously controlled, the combination of several geometric/angular constraints opens new rational design opportunities.<sup>[32]</sup>

## 2.4. Trivalent Metals and New Building Blocks

With the exception of rare-earth (RE) MOFs, which crystallize relatively easily,<sup>[27]</sup> the reactivity of other trivalent metals has been an obstacle to their early exploration in MOF chemistry, due to predominance of oxides and hydroxides over a wide pH range.<sup>[48]</sup> However, their scarcity is balanced by their usually high chemical stability, and in time, notable examples with exceptional properties have been developed, such as the mesoporous MIL-100<sup>[49]</sup> and MIL-101,<sup>[50]</sup> MOFs with zeolitic topologies. In addition, MOFs with fascinating breathing properties<sup>[51,52]</sup> have been developed (MIL-53,<sup>[53]</sup>

MIL-88A<sup>[34]</sup>), which maintain crystallinity upon more than 200% swelling.

### 2.5. Tetravalent Metals and High Connectivity

Given the notable overall increase of chemical stability exhibited by MOFs based on M<sup>III</sup> clusters/chains, the MOF community naturally explored the potential of tetravalent metal carboxylate MOFs, such as zirconium<sup>[29]</sup> and titanium.<sup>[54]</sup> As expected, many of these long-awaited materials exhibit improved chemical and hydrothermal stability,<sup>[55]</sup> initiating the study of their potential for water harvesting.<sup>[56]</sup>

### 2.6. Modulator, a “Major Cornerstone”

While the right balance between nucleation and growth had been identified early on for MOFs based on divalent metals such as Zn and Cu, it remained a major challenge to elucidate the structure of several M<sup>III</sup> (Cr, Al) and M<sup>IV</sup> (Ti, Zr) MOFs.<sup>[49]</sup> In order to control the reaction kinetics of metals with high reactivity, therefore allowing for crystal growth, a modulation approach was developed, using monotopic agents to stabilize the targeted MBBs, thus inducing a regulated exchange/competition with the organic polytopic ligand. While formic acid had already been used in the synthesis of early carboxylate MOFs,<sup>[24]</sup> its widespread implementation in the field took years. Wisely utilized, formic acid permits controlled anisotropic growth.<sup>[57]</sup> It was the key to growing Zr-MOF single crystals,<sup>[58]</sup> thus making it possible to take advantage of the versatility of the Zr-hexanuclear MBB.<sup>[59]</sup>

Finally, it has been found that some specific modulators not only help in the growth of single crystals, but are in fact mandatory for the in situ formation of specific clusters,<sup>[60]</sup> even allowing the discovery of new ones.<sup>[61]</sup>

### 2.7. The Quest for New and Higher Connectivities

The use of polynuclear clusters clearly marked a step in the rational design of MOFs, providing access to MBBs of higher connectivities and directionality.<sup>[62]</sup> As the number of possible nets is restricted when the connectivity of the nodes increases, achieving high connectivity not only makes it possible to target previously unattainable nets, but also limits the number of possible outcomes, which is a prerequisite to promote and achieve rational design.

In recent years, several highly connected MBBs have been unveiled with connectivity higher than 8. These can have 12 connected cuboctahedral (Zr,<sup>[29]</sup> Hf,<sup>[63]</sup> Ti,<sup>[54]</sup> RE<sup>[60]</sup>), hexagonal prismatic (RE,<sup>[64]</sup> Zr,<sup>[65]</sup> Np<sup>[66]</sup>) directionality, or higher connectivity such as 18<sup>[61]</sup> or even 24.<sup>[67]</sup>

### 2.8. Derived Nets and Ligand Diversity

The quest for highly connected MOFs stimulates researchers' creativity; when a specific geometry does not exist in the MBB catalogue, or is yet to be discovered, it is often possible, by means of derived and related nets,<sup>[42]</sup> to find alternative ways to reach the overall expected topology.

While from a pure topological point of view, many materials exhibit a derived net topology, it is widely accepted/recommended to name them after the parent net that provides the main information for design needs. Some relevant examples are the **soc**-MOFs (formally **edq**), many **nbo**-MOFs (**fof**, derived from **nbo-b**), and **rht**-MOFs (**ntt**).<sup>[41]</sup>

### 3. Multicomponent MOFs

Frameworks incorporating multiple components can be divided into two distinct classes, multivariate MOFs (MTV-MOFs) and multicomponent MOFs (Figure 3). Multicomponent MOFs, which are well-ordered systems with periodic pore architectures, constructed from multiple linkers which are topologically distinct from one another (in terms of length and connectivity), often bearing differing functional groups.<sup>[68,69]</sup> Multicomponent MOFs can be distinguished individually in a crystalline lattice. As a result, multiple functionalities are positioned in predefined areas within a MOF pore. Crystallographic and positional order are addressed during framework growth, where the arrangement of the different linkers and their respective spatial orientation can be achieved.<sup>[68]</sup>

Careful control over the reaction conditions is necessary in multicomponent MOF synthesis to hinder the formation of competing phases, specifically when solvothermal synthetic methods are employed. UMCM-1 ([Zn<sub>4</sub>O(bdc)(btb)<sub>4/3</sub>] (btb = benzene-1,3,5-tribenzoate) is a ternary MOF built from three topologically distinct linkers (one ditopic and two tritopic) and a basic zinc oxide SBU, resulting in a **muo** topology giving both mesopores and micropores.<sup>[70]</sup> However, minor changes in synthetic conditions (i.e., incorrect linker ratio and/or solvothermal reaction conditions) can lead to the formation of the thermodynamically favored, competing single-component phases, MOF-177 and MOF-5.<sup>[70]</sup> This was postulated to set a synthetic limitation on the complexity of multicomponent MOFs offering several linker combinations. However, recent advances in this area have seen the emergence of quaternary and quinary MOFs with three and four distinct linkers, respectively.<sup>[68,71–74]</sup>

The ability to further tune specific building blocks at predicted lattice positions in the MOF delivers a strategy to expand the range and complexity of porous materials for modern applications. MUF-77 ([Zn<sub>4</sub>O(bdc)<sub>1/2</sub>(bpdc)<sub>1/2</sub>(hmt)<sub>4/3</sub>] (bpdc = 4,4'-biphenyl dicarboxylate, hmt = 5,5',10,10',15,15'-hexamethyltruxene-2,7,12-tricarboxylate)), a quaternary MOF with an **ith-d** topology, has small, tetrahedral pores that can be primed as selective heterogenic catalytic sites. Through judicious positioning of functional groups on the three distinct linkers, the small tetrahedral pore in MUF-77 was found to act as a highly competitive

heterogenic catalyst for Aldol reactions while repressing the competing Henry reaction.<sup>[75]</sup> Recently, the shorter ditopic linker (bdc) in MUF-77 was replaced with cubane-1,4-dicarboxylate (cdc) to generate CUB-30. Both linkers exhibit the same metrical spacing of their carboxylate functionalities; however, the cdc linker has greater steric bulk due to its 3D geometry. This endowed CUB-30 with exceptional separation characteristics, making it the first MOF to selectively separate cyclohexane from azeotropic cyclohexane/benzene mixtures.<sup>[73]</sup>

Multicomponent MOFs can also be constructed by incorporating multiple inorganic clusters (or SBUs) into one framework. The resulting MOFs have interesting frameworks and high catalytic activities, but they are more difficult to generate due to the sensitivity of SBU formation to the synthetic conditions.<sup>[68]</sup> Recently, a quaternary MOF system was realised with the combination of Cu-based triangular nodes and Zn-based octahedral and square-planar nodes to give an overall **ott** topology.<sup>[76]</sup>

More recently, a multicomponent MOF was developed with both multiple metal clusters and multiple organic linkers. FDM-8 is a quinary MOF and comprises three distinct organic

linkers (carboxylate- and pyrazolate-based) and two distinct metal clusters (Cu<sup>I</sup> and Zn<sup>II</sup>),  $[(Zn_4O)_3(Cu_5(PyC)_3)_4(bdc)_2(ndc)]$  PyC = 4-pyrazolecarboxylate, ndc = 2,6-naphthalenedicarboxylate). As mentioned earlier, a significant challenge in multicomponent MOF synthesis lies in the co-crystallization of competing thermodynamic MOF phases. If one considers only two of the five components used for FDM-8, one obtains 70 MOF structures that are crystallographically unique, with numerous more possible. Remarkably, the solvothermal synthesis involving all five components results in the exclusive assembly of FDM-8 in pure form.<sup>[72]</sup>

#### 4. Multivariate MOFs

While the rational design of framework structures has undoubtedly contributed to the rapid development of reticular chemistry, it has also set an intrinsic limit on the diversity of their structures and properties. When drawing inspiration from biological systems, it becomes apparent that the introduction of complexity onto an ordered backbone (e.g., DNA, RNA, peptides) is central to the sophistication of their

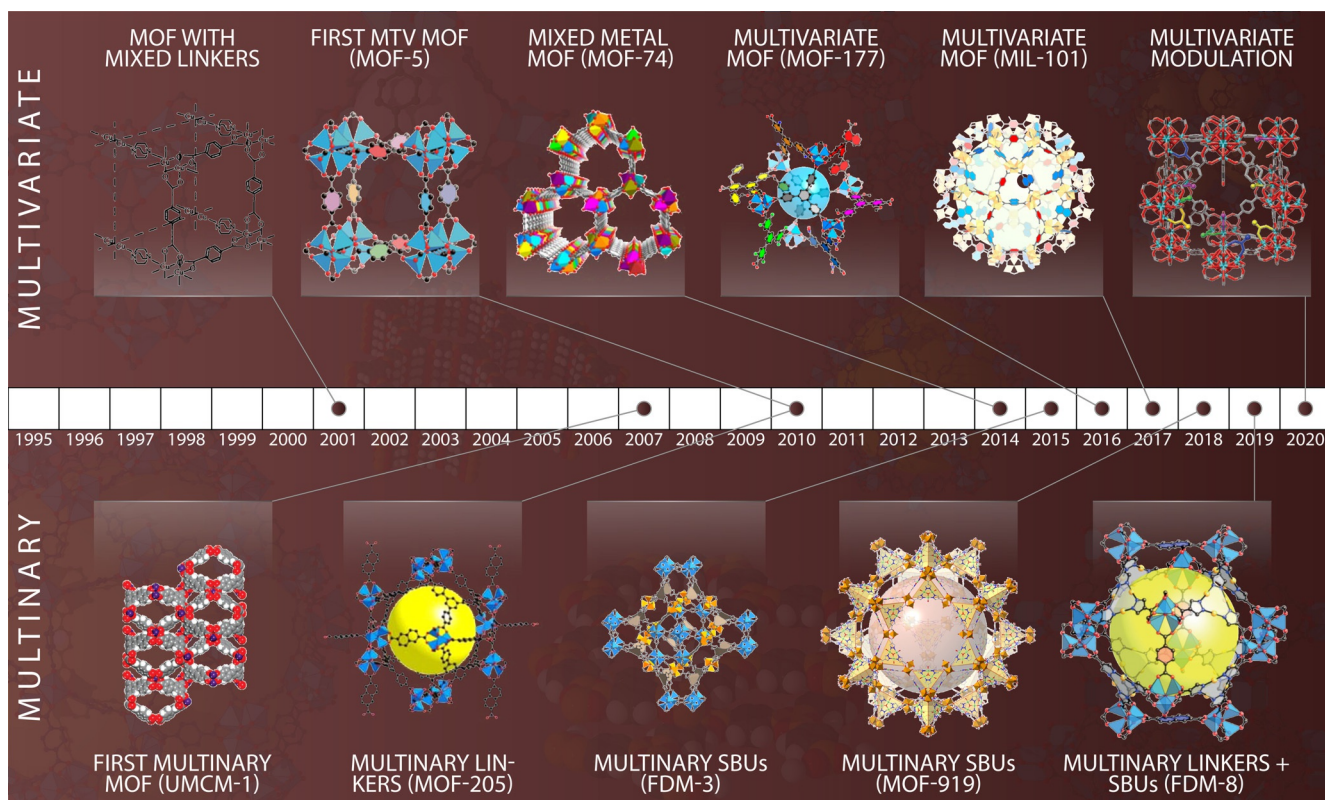


**Figure 3.** Illustrative timeline of the milestones in multicomponent and multivariate MOFs. MOF with mixed linkers (reproduced with permission from ref. [77], Copyright 2001 Chemical Society of Japan). First multinary MOF (UMCM-1) (reproduced with permission from ref. [78], Copyright 2012 Royal Society of Chemistry). First MTV MOF (MOF-5) (reproduced with permission from ref. [79], Copyright 2017 Oxford University Press). Multinary linkers (MOF-205) (reproduced with permission from ref. [80], Copyright 2015 American Chemical Society). Mixed-metal MOF (MOF-74) (reproduced with permission from ref. [81], Copyright 2014 American Chemical Society). Multinary SBUs (FDM-3) (reproduced with permission from ref. [76], Copyright 2015 American Chemical Society). Multivariate MOF (MOF-177) (reproduced with permission from ref. [82], Copyright 2015 American Chemical Society). Multivariate MOF (MIL-101) (reproduced with permission from ref. [83], Copyright 2017 American Chemical Society). Multinary SBUs (MOF-919) (reproduced with permission from ref. [84], Copyright 2018 American Chemical Society). Multinary linkers + SBUs (FDM-8) (reproduced with permission from ref. [72], Copyright 2019 Wiley-VCH). Multivariate modulation (reproduced with permission from ref. [85], Copyright 2020 Wiley-VCH).

function.<sup>[86]</sup> As such, the development of strategies that retain the precision with which the structure of reticular materials can be controlled while allowing for a high level of complexity is paramount. This challenge has been addressed with the discovery of multivariate MOFs,<sup>[86,87]</sup> where “heterogeneity within order” is achieved by introducing variance in functionality (e.g., appended functional groups, metal ions, or vacancies) without altering the underlying backbone of their structure (Figure 3).

#### 4.1. Heterogeneity in Linkers

First steps to increasing the complexity of MOFs by incorporating multiple linkers within one structure date back to as early as 2002 and the discovery of a pillar-layered MOF with the formula  $\text{Cu}_2(\text{pzdc})_2(\text{dpyg})$  (pzdc = pyrazine-2,3-dicarboxylate; dpyg = 1,2-di(4-pyridyl)-glycol).<sup>[88]</sup> In this framework, the two distinct linkers occupy two crystallographically distinct positions, making it the first multicomponent MOF. In contrast, the first multivariate (MTV) MOF was achieved by the incorporation of up to eight distinct linkers (terephthalate and its -NH<sub>2</sub>, -Br, -(Cl)<sub>2</sub>, -NO<sub>2</sub>, -(CH<sub>3</sub>)<sub>2</sub>, -C<sub>4</sub>H<sub>4</sub>, -(OC<sub>3</sub>H<sub>5</sub>)<sub>2</sub> and -(OC<sub>7</sub>H<sub>7</sub>)<sub>2</sub> derivatives) within one pure phase of MOF-5. In the crystal structure, the linkers are mutually interchangeable, leading to a heterogeneous arrangement of appended functional groups throughout the ordered backbone of the framework.<sup>[89]</sup> Importantly, this multivariate framework displayed a  $\approx 400\%$  enhancement in selectivity for sorption of CO<sub>2</sub> over CO compared to its single-linker analogues. The generality of such synergistic effects was confirmed for MTV MOF-177, where a 25% increase in volumetric H<sub>2</sub> uptake over linear combinations of single-linker analogues was observed.<sup>[82]</sup> A direct consequence of multivariate linker arrangements is that host-guest interactions can be tuned continuously by modulating the ratios of their constituents. This was illustrated for MTV MIL-101, where the ratio of two functionalized linkers was incrementally tuned between 0% and 100%. In this way, the interaction of the resulting MTV frameworks with guest molecules (i.e., ibuprofen, rhodamine B, and doxorubicin) could be modulated.<sup>[83]</sup>

#### 4.2. Heterogeneity in Metals

MTV MOFs can also be achieved by mixing metals within the inorganic SBUs. The challenge in making these frameworks lies in the fact that reticulating more than one type of metal precursor often results in the synthesis of mixed MOF phases rather than a single mixed-metal MTV MOF. To overcome this issue, metals must be chosen carefully, such that they can form the same SBU under identical reaction conditions. This was demonstrated first for mixed-metal MTV MOF-74, in which 2, 4, 6, 8, and 10 kinds of divalent metals (Mg, Ca, Sr, Ba, Mn, Fe, Co, Ni, Zn, and Cd) were introduced into a pure single-phase structure.<sup>[80]</sup> Multimetal MTV MOFs can also be realized in discrete SBU frameworks. To this end, mixed-metal MOFs comprising M<sub>3</sub>O trigonal

SBUs (Mn<sub>x</sub>Fe<sub>3-x</sub>O, Ni<sub>x</sub>Fe<sub>3-x</sub>O, Co<sub>x</sub>Ni<sub>3-x</sub>O, Mn<sub>x</sub>Co<sub>3-x</sub>O, Mn<sub>x</sub>Mg<sub>3-x</sub>O, and Mn<sub>x</sub>Ni<sub>3-x</sub>O) and tetrakis(4-carboxyphenyl)-porphyrin linkers were synthesized.<sup>[90]</sup>

#### 4.3. Heterogeneity through Postsynthetic Modification

Postsynthetic modification, as outlined in Section 9, can be applied to introduce functionality into the backbone of MOFs and COFs. Generally speaking, such transformations do not go to full completion and as such inevitably lead to heterogeneity. This approach has been exploited in the generation of MOFs with both functionality and metal heterogeneity.<sup>[91,92]</sup> One particularly impressive example is the successful modification of MTV IRMOF-74-III through seven postsynthetic reactions to covalently incorporate tripeptides, whose spatial arrangement resemble the active site of enzymes, into its pores.<sup>[91]</sup> The heterogeneous pore environment thus achieved was shown to catalyze reactions that were previously accomplished only by enzymes.

#### 4.4. Heterogeneity in Vacancies

A special case of heterogeneity within order are vacancies of either organic linkers or inorganic SBUs in frameworks. In the synthesis of UiO-66, modulators such as acetic and formic acid are added to the reaction mixture to improve crystallinity. Inevitably, these modulators compete with organic linkers for coordination sites in the SBUs and thus create linker vacancy defects in the structure (up to  $\approx 10\%$  in UiO-66), while the underlying topology of the framework is retained and it crystallizes in a single phase.<sup>[93]</sup> In an analogous approach, heterogeneity in vacancies can be targeted in a systematic fashion by purposefully doping in linkers of lower topicity, resulting not only in missing organic linkers but also in inorganic SBU vacancies.<sup>[94]</sup>

### 5. Synthesis of COFs

Over the course of the 20<sup>th</sup> century, the understanding of covalent bonding in organic molecules elevated organic synthesis from a purely empirical to a fully rational field of research. In contrast, covalently linked organic macromolecules, with the exception of linear 1D polymers, remained largely undeveloped. It is instrumental to consider the fundamental prerequisites for the rational formation of extended organic materials: 1) their synthesis must be carried out under conditions that maintain the integrity of the molecular precursors, but 2) allow for the reaction to be under thermodynamic control (i.e., with microscopic reversibility) to afford crystalline product. In this context, crystallinity is not merely a means of characterization but instead the direct consequence of phase purity and definitiveness of structure. This challenge was addressed with the development of COFs, by identifying reaction conditions under which this reticulation occurs with thermodynamic control, thus provid-

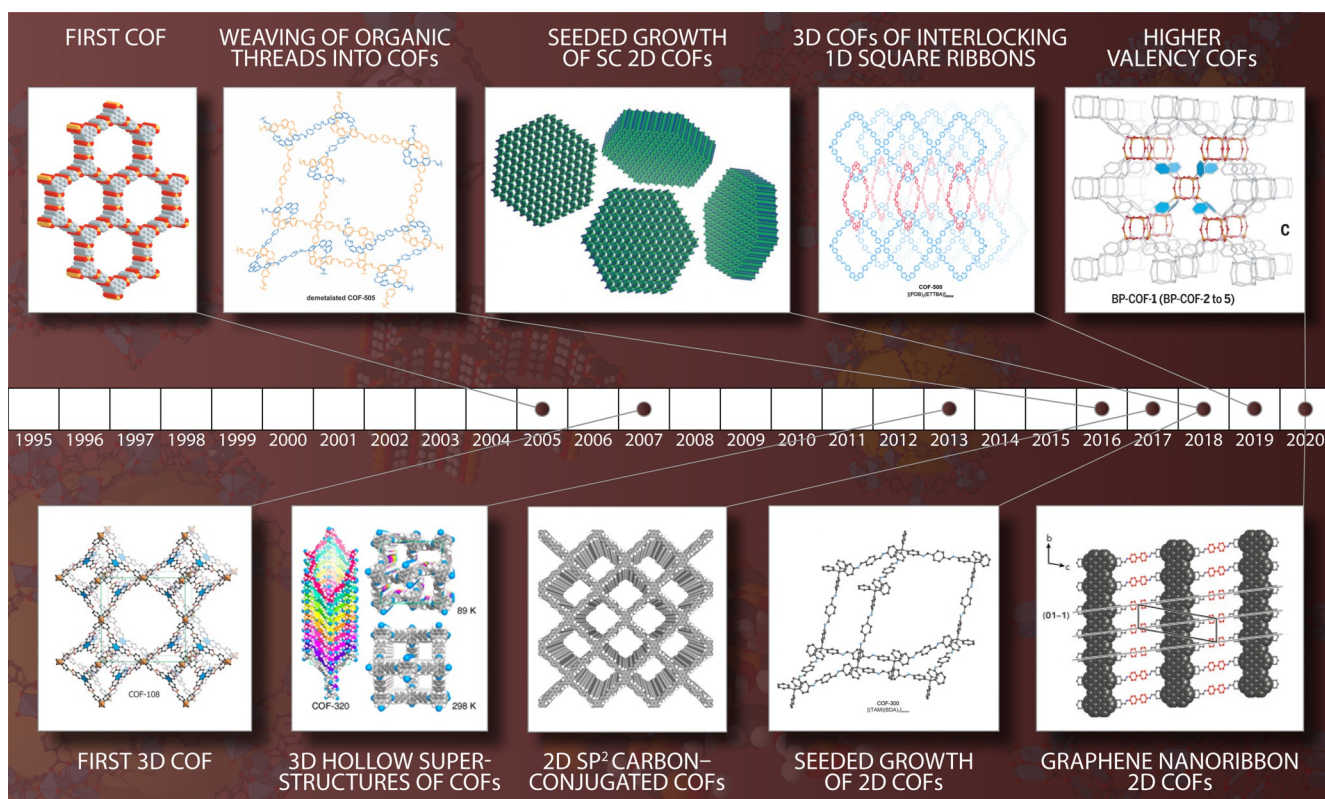


**Figure 4.** Illustrative timeline of the milestones in COF synthesis. First COF (reproduced with permission from ref. [15], Copyright 2005 The American Association for the Advancement of Science). First 3D COF (reproduced with permission from ref. [16], Copyright 2007 The American Association for the Advancement of Science). 3D hollow superstructures of COFs (reproduced with permission from ref. [95], Copyright 2013 American Chemical Society). Weaving of organic threads into COFs (reproduced with permission from ref. [96], Copyright 2016 The American Association for the Advancement of Science). 2D  $sp^2$  carbon-conjugated COFs (reproduced with permission from ref. [97], Copyright 2017 The American Association for the Advancement of Science). Seeded growth of sc 2D COFs (reproduced with permission from ref. [98], Copyright 2018 The American Association for the Advancement of Science). First sc-XRD of COFs (reproduced with permission from ref. [99], Copyright 2018 The American Association for the Advancement of Science). 3D COFs of interlocking 1D square ribbons (reproduced with permission from ref. [100], Copyright 2018 American Chemical Society). Higher valency COFs (reproduced with permission from ref. [101], Copyright 2020 The American Association for the Advancement of Science). Graphene nanoribbon 2D COFs (reproduced with permission from ref. [102], Copyright 2020 Elsevier Inc.).

ing the prerequisite microscopic reversibility for isolating them in crystalline, phase-pure form (Figure 4).

### 5.1. 2D and 3D COFs

The synthesis of the first COFs was achieved through reversible formation of boroxine and boronate ester bonds. Specifically, self-condensation of 1,4-phenylenediboric acid (bdba) or its co-condensation with 2,3,6,7,10,11-hexahydroxyterphenylene (hhtp) yielded COF-1 and COF-5, respectively.<sup>[15]</sup> It must be noted that the stacking of layers in the 2D frameworks is not controlled by covalent bonding but by noncovalent  $\pi$ - $\pi$  interactions. Consequently, control of the stacking is more difficult to achieve. This is illustrated by the fact that COF-1 assumes a staggered stacking conformation, whereas in COF-5 the layers are eclipsed.

In analogy to the reaction conditions used in the formation of 2D COFs, 3D structures were targeted via the formation of boronate ester bonds. Here, condensation of tetra(4-dihydroxyborylphenyl)methane (tbpm) or tetra(4-

dihydroxyborylphenyl)silane (tbps) yielded 3D frameworks COF-102 and COF-103 with underlying **ctn** topology. Cross-condensation of hhtp with tbpm or tbps gave the crystalline 3D framework COF-108 (**bor** topology) and COF-105 (**ctn** topology), respectively.<sup>[16]</sup> In the 15 years following the discovery of 2D and 3D COFs, a myriad of new structures were reported based on a wide variety of linkage chemistries, structure types, and pore metrics. While the structural diversity and reticulation chemistry has developed further since these initial accounts, the fundamental design principles have remained the same. A target structure type is identified and is decomposed into its fundamental geometric units. Equivalents of these geometric units are found in molecules and the necessary functional groups for reticulation appended to their backbone. Finally, reaction conditions are identified under which the constituents can be linked with sufficient microscopic reversibility to enable crystallization and thus unambiguous structural characterization.<sup>[14]</sup>

## 5.2. Linkage Chemistry

A variety of covalent reactions have been adapted to the formation of COFs. One major class of COF linkages are the aforementioned boron–oxygen bond-forming condensation reactions including boroxine, boronate ester, borosilicate, spiroborate, and borate formation.<sup>[15,103,104]</sup> One class of reactions that has been developed is the Schiff base chemistry of imines, hydrazones, and squaraines.<sup>[105–107]</sup> For these reactions, an acid catalyst is required for crystallization. Consequently, the chemical stability of these COFs in the absence of catalyst is substantially enhanced. To further increase their stability, Schiff base chemistry can be coupled to subsequent tautomerization ( $\beta$ -ketoenamine)<sup>[108]</sup> or aromatization (phenazine)<sup>[109]</sup> steps. Finally, *in situ* and *ex situ* strategies for postsynthetic transformation of imine linkages have been developed, giving rise to chemically stable amides (oxidation),<sup>[110]</sup> amines (reduction),<sup>[111]</sup> and benzoxazoles and benzothiazoles (linker exchange followed by oxidative cyclization).<sup>[112]</sup> While those two classes of reactions account for the majority of COFs reported to date, a number of other chemistries have been developed including borazine, imide, acrylonitrile formation, and triazine formation.<sup>[113–115]</sup>

## 5.3. Overcoming the Crystallization Problem

For a long time, one of the major challenges of COF research has been that their small crystallite size precluded solving their structures by single-crystal X-ray diffraction and researchers had to rely on PXRD for structure determination. Since the majority of COFs are imine and boronate ester linked, much effort has been devoted to obtaining sufficiently large crystals for these frameworks. First, the structure of the **dia** topology imine-linked COF-320 was solved by electron diffraction, proving for the first time the single-crystallinity of nanosized COF crystals.<sup>[95]</sup> To slow down the nucleation and prolong precipitation, aniline was added to the imine COF reticulation mixture. This addition converted aldehyde starting materials into imines, which subsequently formed imine COFs through slow transamination as opposed to the faster imine formation. Based on this strategy, the single-crystal structures of three **dia** topology imine COFs (COF-300, COF-303, and LZU-70), as well as one **lon** topology framework (LZU-111) could be solved.<sup>[116]</sup> The latter highlights the importance of single-crystal structure determination of COFs, as the binary and 3-fold interpenetrated **lon** (lonsdaleite) net of the structure is not the default topology and would therefore have been difficult to unambiguously confirm using PXRD.

## 5.4. Increasing the Connectivity

Another challenge in COFs is the limitation in the connectivity of their constituent building blocks, which severely limits their structural diversity compared to MOFs. This holds particularly true for 3D COFs, which are mostly constructed from (poly)aromatic building blocks that gener-

ally favor the formation of layered 2D structures. The main strategy to favor the formation of 3D frameworks in COFs has been the use of tetrahedral building blocks (e.g., based on tetramethylmethane). Consequently, the vast majority of 3D COFs are of **dia**, **bor**, **ctn**, and **pts** topology—the default topologies for the linking of tetrahedra with linear linkers, triangular linkers, and square-planar linkers, respectively.<sup>[14]</sup> In contrast, the large variety of connectivity and shapes of inorganic SBUs in MOFs allow for more diversity in 3D structures. To emulate this, organic SBUs with high connectivity have been targeted. One such strategy is based on linking of trigonal-prismatic shape-persistent organic cages having six pendant amine groups with linear aldehyde linkers into a framework with an interpenetrated **acs** topology.<sup>[117]</sup> Extensive research efforts have been devoted to the synthesis of shape-persistent organic cage molecules, thus giving a number of additional candidates for analogous cage COFs. The disadvantage of the use of shape-persistent cages as SBUs lies in the fact that they are themselves formed by dynamic bond formation, thus complicating their use in COF formation due to the potential for their simultaneous deconstruction. Even when organic cages are stable under COF-forming reaction conditions, they must still be synthesized at large scale prior to COF formation, which makes the entire process laborious and time consuming. For MOFs, the formation of SBUs generally occurs *in situ*, and establishing an analogous methodology for COFs would be beneficial. One such strategy has been developed for the reticulation of 1,4-boronophenylphosphonic acid. Self-condensation of the linker leads to the *in situ* formation of  $B_4P_4O_{12}$  cube SBUs with eight points of extension and the reticulation into a 3D COF with underlying **bcu** topology.<sup>[101]</sup> Finally, linear SBUs with infinite points of extension have been achieved by linking benzaldehyde-functionalized **cove** type polymeric graphene nanoribbons with linear benzidine linkers to form an extended 2D framework.<sup>[118]</sup>

## 5.5. Molecular Weaving

One unique type of linkage that has been developed based on COF chemistry is mechanical bonding. This was first established for COF-505, a three-dimensional framework constructed by interlacing organic threads at regular intervals to form a 3D **dia** material. Practically, this was achieved by linking tetrahedral aldehyde-functionalized  $Cu(PDB)_2(BF_4)$  (copper(I)-bisphenanthroline tetrafluoroborate) with bz (benzidine) linkers. Here, the copper centers serve as templates for the formation of the targeted woven arrangement (as opposed to the favored parallel arrangement) and can be reversibly removed following reticulation. Removal results in a tenfold increase in elasticity of the material, highlighting the prospect of woven structures in the design of solids with unprecedented flexibility in the solid state.<sup>[96]</sup> Along these lines, related woven COFs have been shown to incorporate guest molecules that exceed the size of their pores in a process termed adaptive inclusion.<sup>[119]</sup> Linking through mechanical bonding is not restricted to molecular weaving but can also be achieved through the interlocking of rings. The

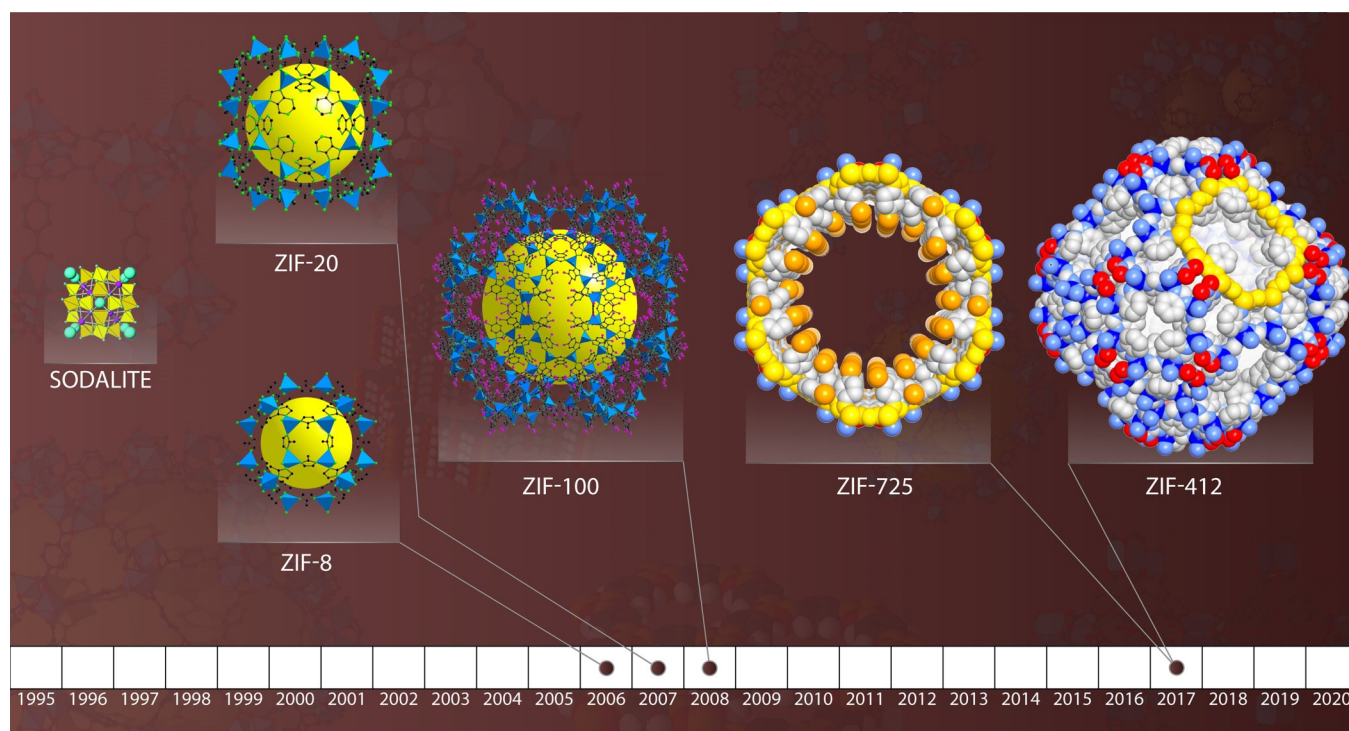


**Figure 5.** Illustrative timeline of the milestones in ZIF synthesis. Sodalite, ZIF-8, ZIF-20, ZIF-100 (reproduced with permission from ref. [128], Copyright 2010 American Chemical Society). ZIF-725, ZIF-412 (reproduced with permission from ref. [129], Copyright 2017 American Chemical Society).

reaction of the  $\text{Cu}(\text{PDB})_2(\text{PO}_2\text{Ph}_2)$  complex with a tetratopic linker yields COF-500 with **pts** topology.<sup>[120]</sup>

## 6. Synthesis of ZIFs

Zeolitic imidazolate frameworks (ZIFs) are a unique subclass of MOFs. Unlike many MOFs made of polynuclear metal nodes and chelating organic linkers, ZIFs are constructed from single metal ions bridged by imidazolate linkers. The choice of particular building units yields especially porous structures, making ZIFs distinctive from other MOFs (Figure 5).

The discovery of ZIFs originates from the idea of introducing zeolitic topologies into MOF chemistry.<sup>[121–127]</sup> In order to create large pores in MOFs, long organic linkers are often required, but they are less synthetically accessible than short, simple ones. Using short linkers to construct large pores is possible when the pore, geometrically a polygon, is enclosed by a high number of faces (or edges); although each edge is short, they can add up to enclose a vast space. This principle can be observed in the structure of zeolites, whose structures serve as a pillar of modern chemical industry. In zeolites,  $\text{Al}^{3+}$  and  $\text{Si}^{4+}$  are connected by  $\text{O}^{2-}$  forming large cages, which in turn encompass void space accessible to desired guest molecules.<sup>[130]</sup> The key structural feature of zeolites is the tetrahedral silicate unit, which shares an O atom at a common vertex, forming a Si–O–Si angle of  $145^\circ$ . This bridging angle precludes the formation of dense structures with the default **dia** topology, and thus allows for a wide range of products with high porosity.

ZIFs emerged as the metal–organic analogue of zeolites, where the tetrahedral  $\text{Al}^{3+}$  and  $\text{Si}^{4+}$  in zeolites are replaced by  $\text{M}^{2+}$  ( $\text{M} = \text{Zn}$  or  $\text{Co}$ ), and  $\text{O}^{2-}$  by imidazolate to connect the metal ions.<sup>[12,131–133]</sup> The two N donors on imidazolate are positioned such that the M–imidazolate–M angle is  $145^\circ$ , a value coinciding with the Si–O–Si angle in zeolites, thus favoring the formation of the tetrahedral topologies and porous structures that can be found in zeolites.<sup>[121,123]</sup> For example, ZIF-8, a prototypical ZIF structure with the chemical formula  $\text{Zn}(\text{2-methylimidazolate})_2$ , has a sodalite topology (**sod**), which is named after the naturally occurring mineral sodalite.<sup>[123,134]</sup> In the structure of ZIF-8, tetrahedral Zn nodes are connected by the 2-methylimidazolate linkers to form 4- and 6-membered rings. These rings are fused along their common edges into a truncated octahedral cage with a diameter of  $11.6 \text{ \AA}$ , which is composed of 24 Zn vertices and 36 imidazolate edges. These cages are further fused into a 3D porous network by sharing their 4-membered rings. More than 240 different topologies have been found in zeolites;<sup>[135]</sup> the combination of tetrahedral metal centers and imidazolate allows access to a vast design space for exploring metal–organic counterparts. Today more than 40 topologies have been achieved in the synthesis of ZIFs, some of which were previously unrealized in zeolites.

Unlike zeolites, the synthesis of ZIFs does not rely on the use of structure-directing agents (e.g., alkylammonium salts) to achieve desired topologies; structure-directing agents often act unpredictably. Instead, synthetic outcomes can be modulated through the judicious choice of substitution groups on the imidazolate linker, allowing for structure tuning by design.<sup>[125,129,136]</sup> Based on a comprehensive examination of

ZIF structures, it has been found that large rings and therefore large cage openings can be potentially achieved by introducing bulkiness to imidazolate.<sup>[129]</sup> Following this design principle, the highly bulky linker 6-bromobenzimidazole was employed for the synthesis of ZIF-725, yielding a ring of 24 Zn nodes and a record-breaking cage opening of 22.5 Å. When targeting a large cage size (large pore volume), it is necessary that tetrahedral structures not only have large rings but more importantly many small rings. Accordingly, a balance must be struck by combining imidazolate linkers with both low and high bulkiness. This is exemplified by the structure of ZIF-412, where the bulky benzimidazole and 4-nitroimidazole linkers lead to the formation of 8- and 12-membered rings, while imidazolate, the less bulky linker, facilitates 4- and 6-membered rings; the four sizes of rings all fuse to form the largest cage known for all porous tetrahedral structures with a diameter of 45.8 Å.<sup>[129]</sup>

Compared with zeolites, ZIFs are amenable to a wider range of functionalization chemistry by virtue of the flexibility with which the organic units can be varied. The 2-, 4-, and 5-positions of imidazolate can be designed to bear functional groups of choice, imparting new properties and functions beyond the scope of zeolite chemistry. The incorporation of hydrophobic functional groups into ZIFs, for instance, enables selective capture of CO<sub>2</sub> under humid conditions.<sup>[137]</sup>

## 7. Characterization of Reticular Materials

The history of MOFs and COFs is firmly grounded on their characterization possibilities. In particular, the understanding of their structures lies at the heart of reticular chemistry as the key source of information for engineering new architectures and emergent properties. This section is concerned with the characterization of the structure of reticular materials as a fundamental aspect for understanding their behavior, and will target specifically their morphology, size, crystal structure, local structure, and porosity (Figure 6).

Morphology and particle size are the most important macroscopic structural aspects and among those that have been studied since the early years of reticular chemistry. Scanning and transmission electron microscopy (SEM and (S)TEM), played a pivotal role among the imaging tools used to reveal morphological features.<sup>[138]</sup> These have been complemented by atomic force microscopy (AFM), whose use in solution made it possible to monitor in situ the evolution of single-crystal morphology during crystal growth.<sup>[139]</sup> While imaging offers an unparalleled level of morphological detail, the study of size and shape distributions requires much larger amounts of particles. In this regard, dynamic light scattering (DLS) and fluorescence correlation spectroscopy (FCS) have been employed to determine the size distribution of particles suspended in liquid media,<sup>[140]</sup> while information on shape anisotropy has been retrieved by small-angle and wide-angle X-ray scattering (SAXS/WAXS).<sup>[141]</sup> In particular, WAXS, often generalized as PXRD, can be used to distin-

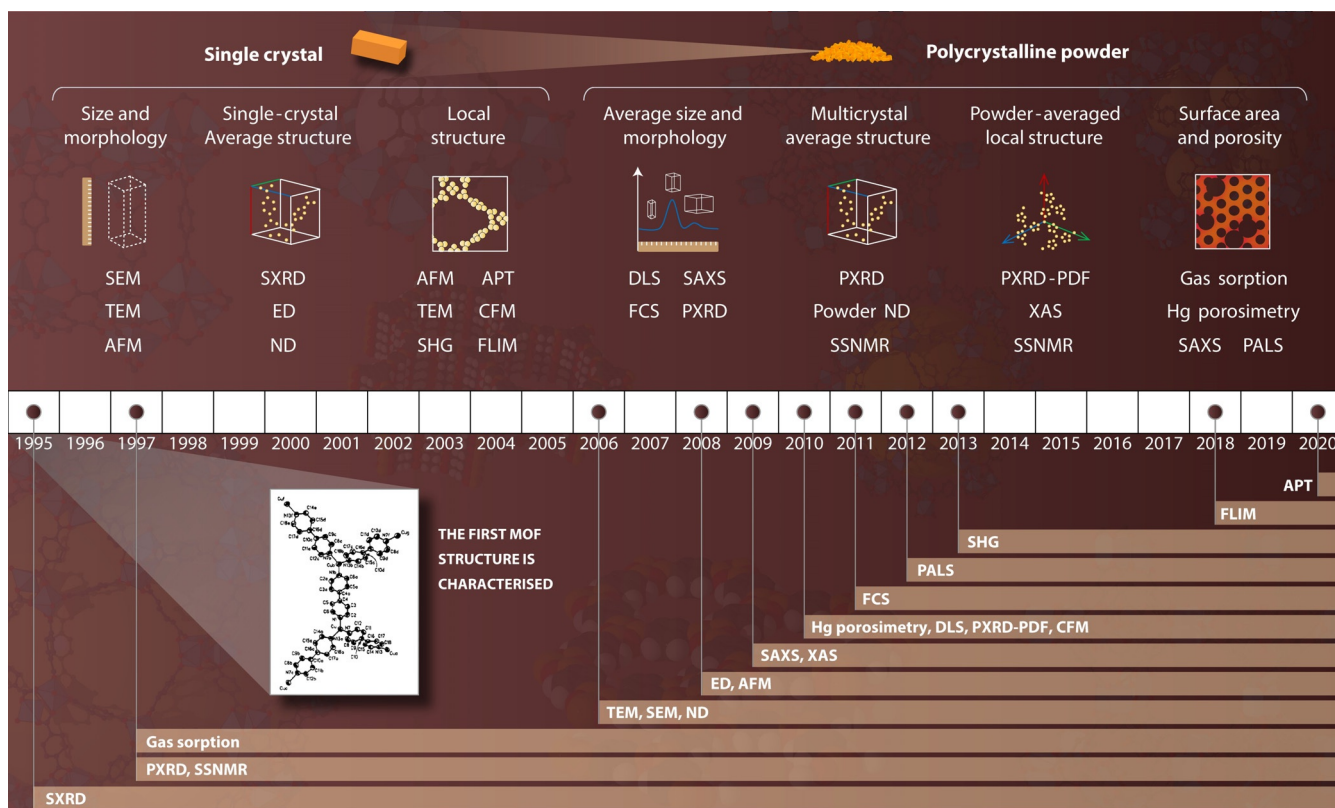


Figure 6. Illustrative timeline of the milestones in the characterization of reticular materials.

guish sizes of particles from those of crystal domains. Although these sometimes coincide, MOFs and COFs often grow in polycrystalline aggregates that behave as single particles in DLS and FCS experiments, and whose single-crystal characteristics can seldom be assessed by microscopy. In these cases, an expert use of the Scherrer equation on PXRD data makes it possible to refine the crystal size distribution, thus complementing the information acquired by other scattering and microscopy analyses.<sup>[140]</sup>

The average structure, also known as crystal structure, is largely considered the most crucial information to acquire for MOFs and COFs. Regardless of whether the material is made of (nearly) periodic crystals or defective domains, the structure of a conceptual unit cell resulting from averaging every unit cell in the sample—the average unit cell—can be derived from the Bragg peaks measured in diffraction experiments. With over a century of history and constant technological and methodological development, single-crystal X-ray diffraction (SXR) remains the gold standard for accuracy in crystal structure determination. Since the beginnings of reticular chemistry, crystal structure analysis relied on SXR, provided suitably large domains can be isolated.<sup>[142]</sup> This size requirement, once several tens of microns, nowadays reaches down to a few microns when synchrotron radiation is used and this lower limit is expected to decrease further with future sources and detectors. While PXRD has been used to provide often less accurate yet more representative information on polycrystalline samples, it has been also employed for *ab initio* structure determination when SXR was not feasible because the crystals were too small or intergrown.<sup>[143]</sup> This solution remained the best available, until the establishment of low-dose electron diffraction (ED) revolutionized the field of single-crystal diffraction analysis. While the strong interactions between electrons and sample causes problematic non-kinematical scattering that keeps the quantitative accuracy of ED below that of SXR, the crystal size of MOFs and COFs became a rare problem, as quasi-parallel electron beams can reach wavelengths of even a few nanometers, thus making it possible to illuminate small domains as well as parts of polycrystalline aggregates.<sup>[144]</sup>

Quite the opposite occurs in neutron diffraction (ND), which generally requires single crystals in the size range 0.5–1.0 mm due to the scarce brilliance of neutron sources. Nevertheless, neutrons offer unique possibilities due to the radically different trend of their scattering cross sections, which unlike those of electrons and X-rays, do not strongly decrease with lower atomic numbers. This allows light and heavy elements to contribute similarly to diffraction patterns, and for this reason powder ND has been employed on polycrystalline MOFs to study host–guest interactions involving H<sub>2</sub>, CH<sub>4</sub>, and CO<sub>2</sub>.<sup>[145–147]</sup> Besides diffraction techniques, solid-state nuclear magnetic resonance spectroscopy (SSNMR) on polycrystalline powders has also entered reticular chemistry as a useful crystallographic tool with the advantage of discriminating between different elements in the crystal.<sup>[148]</sup>

While the average structure is a useful simplification allowing for a general description of MOFs and COFs, their properties can be rationalized only when their actual struc-

ture is known. Nearly perfect crystals can sometimes be reasonably approximated as a periodic repetition of a single unit cell model, but often the more sophisticated structures of MOFs and COFs are only properly understood once their spatially varying features such as disorder, defects, or dynamics are unravelled. Local structural information has been obtained either as absolute and relative to a very restricted region of a crystal or averaged over all crystals in a powder sample. Absolute local structure can be achieved by microscopy or tomography techniques, traditionally (S)TEM<sup>[149]</sup> and AFM,<sup>[150]</sup> but also by second harmonic generation (SHG) microscopy,<sup>[151]</sup> confocal fluorescence microscopy (CFM),<sup>[152]</sup> fluorescence lifetime imaging microscopy (FLIM)<sup>[153]</sup> and atom probe tomography (APT).<sup>[154]</sup> Diffraction techniques based on X-rays, electrons, and neutrons are useful to investigate not only crystal structures, but also powder-averaged local structures. In fact, diffuse scattering distributed between the Bragg positions always populates the diffraction patterns of MOFs and COFs. This scattering component from PXRD data has been used to derive the radial distribution of all atom–atom correlations, known as the pair distribution function (PDF), against which local structure models can be refined.<sup>[155]</sup> Finally, an important role is also played by spectroscopies such as X-ray absorption spectroscopy (XAS) and SSNMR,<sup>[156]</sup> which allow the advantageous isolation of atomic species at which the detected signals originate. It is worthwhile mentioning that these techniques have been particularly crucial in research on amorphous and glassy frameworks as their lack of long-range periodicity makes the local structure their most important crystallographic aspect.

One last structural feature that has always been paramount in the study of MOFs and COFs is porosity. Since the origins of reticular chemistry, nitrogen and argon sorption measurements have remained standard practice due to their long-time methodological development and wide availability.<sup>[157]</sup> On the other hand, this method strongly relies on theoretical models and approximations, and therefore several complementary techniques have been added to the analytical toolbox for investigating porosity. SAXS analysis is well qualified for this purpose as it provides reliable detection of nanometric porosity variations in bulk polycrystalline samples.<sup>[158]</sup> Porosimetry measurements by mercury intrusion–extrusion cycles can be used to explore porosity while also providing additional information on sample density and pressure-induced mechanical behavior.<sup>[159]</sup> Finally, positron annihilation lifetime spectroscopy (PALS) has been employed to determine the local free volume of framework materials and to unravel the complex porosity of MOF–polymer matrix composites.<sup>[160]</sup>

## 8. Computational Modelling of Reticular Frameworks

Reticular frameworks have opened up an immense chemical space where countless possibilities in their structures, interactions, and applications have been largely undiscovered experimentally. The utilization of computational

power, as a result, is indispensable to the field in exploring this chemical space beyond experimental limitations.<sup>[161]</sup>

This effort involves the modelling and simulation of reticular frameworks, specifically, the building of mathematical models that replicate the framework structures, of which the physicochemical properties, interactions, and dynamics are studied with algorithms derived from known physical principles and chemical knowledge. The aims, as such, include 1) the accurate representation of the structures, 2) the precise calculation of their energy and thus physicochemical properties, 3) the proper simulation of the interactions within frameworks and with guests, 4) the development of affordable computational tools, and 5) their generalized establishment to enable predictive studies of new materials.

### 8.1. Structural Modelling

The accurate representation of the structure of reticular frameworks represents the fundamental basis on which *in silico* simulations become feasible. Benefitting from the crystalline nature, models of reticular frameworks characterized by SXRD or 3D-ED can be built by importing the crystallographic coordinates.<sup>[162, 163]</sup> It is, however, worth

noting that diffraction studies mostly yield periodic, averaged structural information, while reticular structures with disorder, aperiodic defects, and dynamics are inevitably studied with modelling for the accurate representation of local structures. In other cases, where diffraction data are unavailable, *ab initio* structural models are built. This process intellectually benefits from the principle of reticular synthesis,<sup>[1]</sup> in which a selected topology determines the connectivity and symmetry, fragments of SBUs or linkers are superimposed onto the nodes and edges, and linkages are created in between to form extended frameworks, followed by geometric optimization. This process plays a critical role in structure elucidation in such cases. COFs are exemplars where only several single-crystal structures have been reported to date.<sup>[116]</sup> Since the first publication of COFs,<sup>[15]</sup> a routine has been established in which modelled structures are generated as above, and predicted PXRD patterns are compared with experimental PXRD data and finished by whole-pattern powder refinement. Automation of this process has been achieved through custom codes<sup>[164]</sup> and general-purpose packages.<sup>[165]</sup> This enables the generation of hypothetical structures in large quantities which are useful for screening studies (Figure 7).

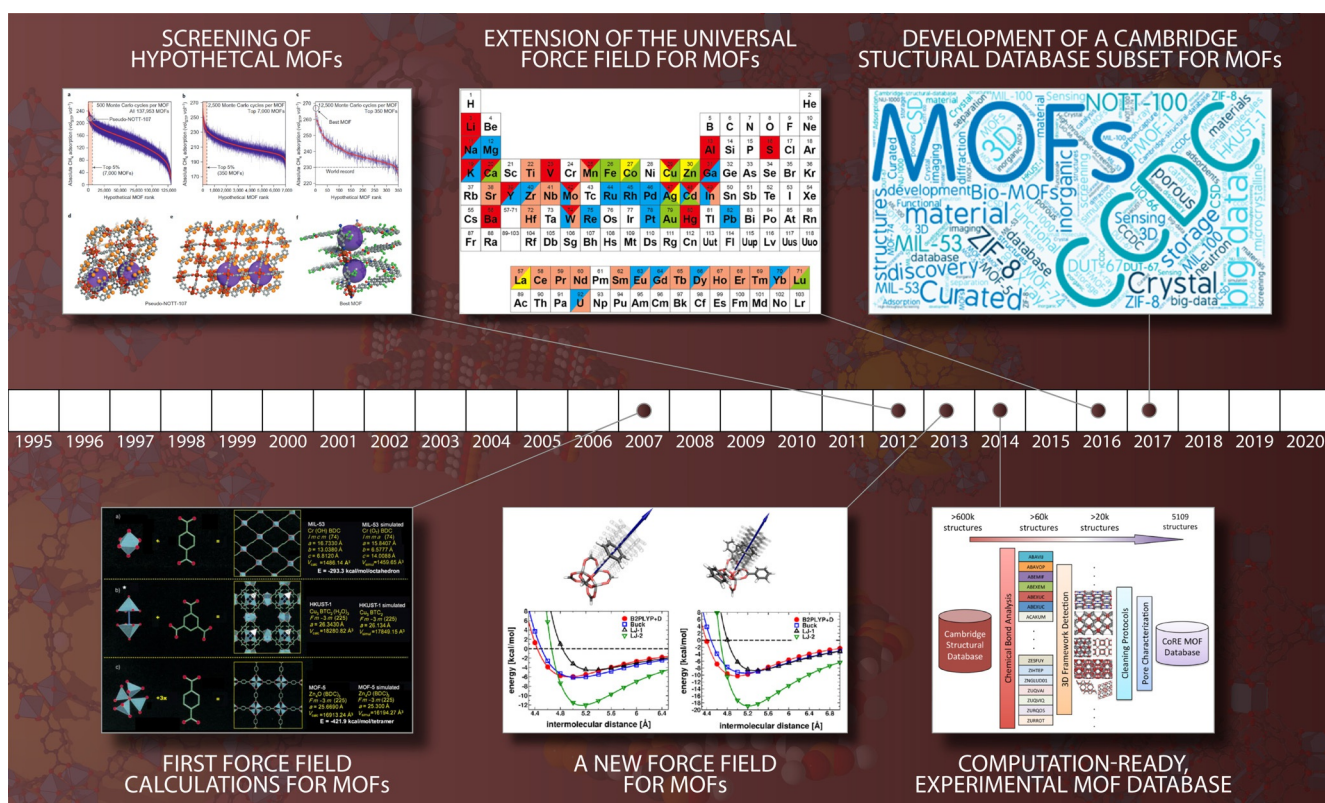


**Figure 7.** Illustrative timeline of the milestones in the computational modelling of reticular frameworks. First force field calculations for MOFs (reproduced with permission from ref. [179], Copyright 2007 Wiley-VCH). Screening of hypothetical MOFs (reproduced with permission from ref. [180], Copyright Springer Nature 2011). A new force field for MOFs (reproduced with permission from ref. [181], Copyright 2013 Wiley-VCH). Computation-ready experimental MOF database (reproduced with permission from ref. [182], Copyright 2014 American Chemical Society). Extension of the universal force field for MOFs (reproduced with permission from ref. [176], Copyright 2016 American Chemical Society). Development of a Cambridge structural database subset for MOFs (reproduced with permission from ref. [183], Copyright 2017 American Chemical Society).

## 8.2. Calculation of Energy and Interactions

The precise calculation of the energy of a model is fundamental for all other simulation studies. The first stage of this research employs existing computational methods at ab initio quantum mechanics (QM), density functional theory (DFT), and molecular mechanics (MM) levels, to address different interactions. QM and DFT on reticular frameworks follow mostly the same principles as on other materials, such as molecular species.<sup>[166]</sup>

Framework–guest interactions, especially non-reactive physisorption where intermolecular forces prevail, can be well handled with molecular mechanics.<sup>[167]</sup> Simulation of framework dynamics upon uptake and removal of guests is also practical to study at this level.<sup>[168]</sup> The forcefields that were first used in these studies were existing ones such as DREIDING,<sup>[169]</sup> UFF,<sup>[170]</sup> and OPLS.<sup>[171]</sup> These served as the basis for the development of new, dedicated potentials and parameters for reticular materials, such as DWES,<sup>[172]</sup> MOF-FF,<sup>[173]</sup> BTW-FF,<sup>[174]</sup> VMOF,<sup>[175]</sup> and UFF4MOF.<sup>[176]</sup> For studies with stronger interactions such as chemisorption or catalysis, hybrid quantum mechanics/molecular mechanics (QM/MM) methods have been employed in reticular materials to achieve a higher level of accuracy while maintaining efficiency.<sup>[177,178]</sup> The simulation of dynamic processes at the MM level includes molecular dynamics (MD) and Monte Carlo (MC). These have been successfully applied in the simulation of processes such as sorption,<sup>[184]</sup> diffusion,<sup>[185]</sup> breathing,<sup>[168]</sup> and framework degradation.<sup>[186]</sup>

## 8.3. Predictive Screening

Once the transferability of the above methods is established, the most exciting aspect of computational studies of reticular materials is possible—the predictive screening of undiscovered materials or hypothetical structures, thus circumventing the challenge of exhaustive experimental synthesis. The Cambridge Structural Database (CSD) has established a dedicated MOF subset to host their crystallographic data,<sup>[183]</sup> while disorder-free, cleaned structure models from these data are built as computation-ready experimental databases.<sup>[187,188]</sup> Hypothetical databases have been generated as well.<sup>[189,190]</sup> Based on these, numerous simulation screening studies have been performed for the prediction of methane<sup>[187]</sup> and hydrogen storage,<sup>[191]</sup> and carbon capture,<sup>[192]</sup> showing considerable agreement with experiments.

## 9. Postsynthetic Modification

The concept of postsynthetic modification (PSM) to chemically functionalize the framework post-assembly was first described in 1990 in the report of an extended 3D coordination solid.<sup>[193]</sup> Although the first demonstrations of PSM were described earlier, active exploration of PSM of MOFs began in the mid-2000s, and since that time has grown substantially. Today, PSM is a routine approach for MOF functionalization that has arguably exceeded the use of direct

MOF functionalization via ligand prefunctionalization (Figure 8).

### 9.1. Early Reports of PSM

In an early example of PSM on the ligands of coordination solids, alcohol-bearing 1,3,5-tris(4-ethynylbenzotrile)benzene ligands were crystallized with Ag<sup>I</sup> to form an open hexagonal lattice. PSM with trifluoroacetic anhydride vapor converted the alcohol to the corresponding ester with retention of the porous structure of the lattice.<sup>[194]</sup> Similar ligands were subsequently treated postsynthetically with silyl triflates, which could not only react with a single alcohol group, but with multiple alcohol groups on different ligands.<sup>[195]</sup> While generally resulting in complex mixtures of products, this experiment demonstrated that PSM could result not only in modification, but also crosslinking, oligomerization, and polymerization of ligands.<sup>[195]</sup>

### 9.2. PSM Emerges

Around the mid-2000s, a number of studies that focused more on the potential for functionalizing and modulating the properties of MOFs brought PSM out of a nearly seven-year hiatus. PSM of IRMOF-3 (comprised of Zn<sup>II</sup> and NH<sub>2</sub>-bdc<sup>2-</sup>) with acetic anhydride yielded the acylated framework IRMOF-3-AM1 (80% conversion), which could not be obtained by direct synthesis.<sup>[196]</sup> Notably, the authors of the aforementioned study coined the term postsynthetic covalent modification (PSM).<sup>[196]</sup> Experiments with anhydrides having alkyl substituents of various lengths showed that there was a steric upper limit for high PSM conversion efficiencies in IRMOF-3 (>80%) at about nine alkyl carbons.<sup>[203]</sup> Further elongation resulted in a substantial drop in conversion (<11%),<sup>[203]</sup> suggesting the possibility of confining PSM to the surface of the MOF crystallites. Such steric effects were subsequently used to render hydrolytically unstable MOFs more stable by making their surface hydrophobic or even superhydrophobic.<sup>[204]</sup> More recent studies have highlighted how solvent choice and reagent reactivity can allow for a high degree of spatial control of PSM within MOF crystals.<sup>[205]</sup>

One limitation of the reported amine-to-amide PSM reactions was the formation of acidic byproducts that could degrade many early MOFs.<sup>[196,206]</sup> As an alternative, the reaction of amino groups with isocyanates and isothiocyanates was developed, which produce (thio)urea linkages without any byproducts.<sup>[207]</sup> Additionally, imine condensations on amine-bearing MOF ligands were reported. For example, the reaction of IRMOF-3 with salicylaldehyde produced the imine condensation product via PSM (13% conversion).<sup>[208]</sup> The resulting salicylidene metal binding sites were subsequently metalated with V(O)acac<sub>2</sub> to yield a catalytically active material for the oxidation of cyclohexene with *t*-BuOOH, laying the foundation for future studies.<sup>[208]</sup>

The use of imine condensation reactions in PSM further suggested the use of aldehydes as versatile chemical handles.<sup>[209]</sup> An aldehyde-tagged analogue of IRMOF-9 was

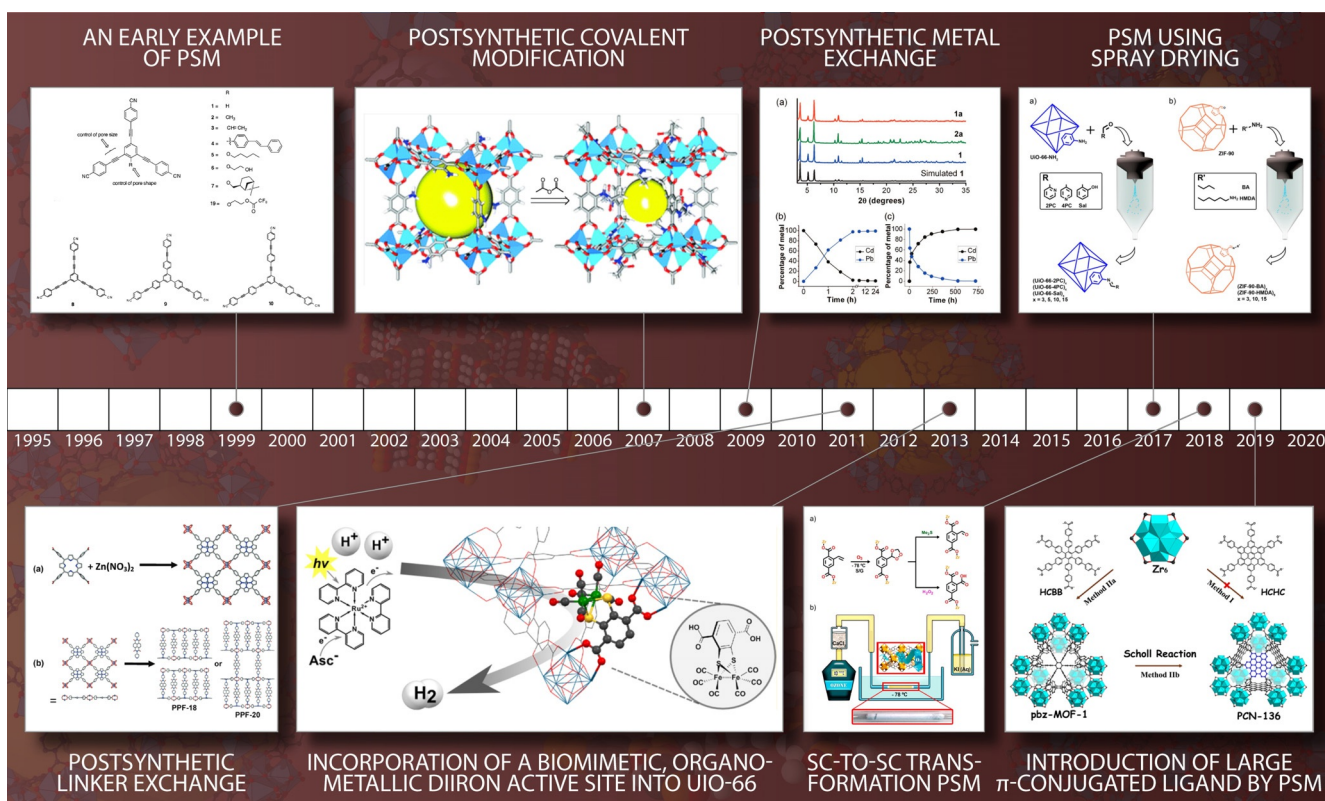


**Figure 8.** Illustrative timeline of the milestones in the postsynthetic modification. An early example of PSM (reproduced with permission from ref. [194], Copyright 1999 American Chemical Society). Postsynthetic covalent modification (reproduced with permission from ref. [196], Copyright 2007 American Chemical Society). Postsynthetic metal exchange (reproduced with permission from ref. [197], Copyright 2009 American Chemical Society). Postsynthetic linker exchange (reproduced with permission from ref. [198], Copyright 2011 American Chemical Society). Incorporation of a biomimetic organometallic diiron active site into UiO-66 (reproduced with permission from ref. [199], Copyright 2013 American Chemical Society). PSM using spray drying (reproduced with permission from ref. [200], Copyright 2017 American Chemical Society). Sc-to-Sc transformation PSM (reproduced with permission from ref. [201], Copyright 2018 American Chemical Society). Introduction of large  $\pi$ -conjugated ligand by PSM (reproduced with permission from ref. [202], Copyright 2019 American Chemical Society).

treated with a substituted hydrazine to produce a hydrazone-functionalized MOF.<sup>[210]</sup> This study was the first to provide crystallographic evidence for PSM. Another early report of the use of aldehyde tags for PSM was achieved with ZIF-90.<sup>[211]</sup> In this study, the aldehyde handle was transformed via PSM by either reduction to the corresponding alcohol with  $\text{NaBH}_4$  or condensation with ethanolamine to produce the resulting imine.<sup>[211]</sup> The modifications resulted in ZIFs with markedly different  $\text{N}_2$  gas sorption isotherms, indicating that PSM could dramatically alter the porosity and gas sorption properties of the resulting framework.

### 9.3. PSM Portfolio

The development of PSM inspired the elaboration of related methods including PSD (postsynthetic deprotection), PSE (postsynthetic exchange), PSP (postsynthetic polymerization), SALE (solvent-assisted linker exchange), SALI (solvent-assisted ligand incorporation), and others. In PSD, instead of introducing a new chemical functionality into the MOF lattice, the chemical handle is removed to uncover an underlying chemical group. Important examples of PSD include the introduction of phenol/catechol groups, free

amines, and alkyne substituents using photoreactive, thermal, and chemical deprotection strategies, respectively.

Alcohols or diols (in the form of phenol or catechol groups) were introduced into UMCM-1 via a photochemically driven PSD reaction.<sup>[212]</sup> Here, the standard  $\text{H}_2\text{bdc}$  ligand was replaced with either 2-hydroxy-1,4-benzenedicarboxylic acid ( $\text{HO-H}_2\text{bdc}$ ) or 2,3-dihydroxy-1,4-benzenedicarboxylic acid ( $\text{CAT-H}_2\text{bdc}$ ,  $\text{CAT}$  = catechol). Because the strong metal-binding capabilities of the  $\text{HO-H}_2\text{bdc}$  and  $\text{CAT-H}_2\text{bdc}$  ligands preclude their direct use in the preparation of UMCM-1, nitrobenzyl-protected versions of these ligands, 2-((2-nitrobenzyl)oxy)terephthalic acid ( $\text{NO}_2\text{BnO-H}_2\text{bdc}$ ) and 2,3-bis((2-nitrobenzyl)oxy)terephthalic acid ( $(\text{NO}_2\text{BnO})_2\text{-H}_2\text{bdc}$ ), were employed. Following formation of the framework, PSD by irradiation at 365 nm afforded the target structure with high conversion efficiency (75–100%), retention of crystallinity, and increased  $\text{N}_2$ -accessible surface areas resulting from the removal of space-filling groups. Exposure of the deprotected framework UMCM-1-CAT to an  $\text{Fe}^{\text{III}}$  source resulted in a color change of the material to deep red purple, showing that the PSD-generated catechol groups are available for metal binding.<sup>[212]</sup>

In another report, thermal deprotection was used to deprotect an amine functional group and free up surface area

within a MOF.<sup>[213]</sup> The attachment of a bulky NHBoc group onto the ligand of an IRMOF-12 derivative prevented framework interpenetration during synthesis (as opposed to the framework with unfunctionalized ligand), thus demonstrating the use of the protecting group to control framework interpenetration. Heating the MOF crystals to 150 °C in DMF lead to PSD by thermolysis in a SCSC fashion.<sup>[213]</sup>

Deprotection can also be achieved chemically, and in a surface-selective manner.<sup>[214]</sup> A pillared paddlewheel MOF was prepared by the combination of 3-[(trimethylsilyl)ethynyl]-4-[2-(4-pyridinyl)ethenyl]pyridine, 2,6-naphthalenedicarboxylic acid, and Zn<sup>II</sup>. Desilylation of the ligands was achieved by treatment with tetrabutylammonium fluoride (TBAF), with the large size of the NBu<sub>4</sub><sup>+</sup> counterion restricting the deprotection to the crystal surface. The produced alkyne groups could be coupled to ethidium bromide monazide (via “click” chemistry) and analysis by fluorescence confocal microscopy showed their localization on the surface of the crystals.<sup>[214]</sup>

Another modification strategy is PSE, versions of which are also frequently referred to as SALI and SALE. PSE reactions involve the replacement of ligands in a postsynthetic manner, and, in the case of SALI, ligand introduction without replacement. In addition to ligands, the exchange (and addition) of metal ions into MOFs by PSE has also been reported.<sup>[215]</sup> PSE has proven to be an incredibly versatile approach for functionalizing MOFs, and has been studied extensively.<sup>[215,216]</sup>

Many of the earliest examples of PSE were demonstrated using metal ions, rather than ligand exchange. Complete SCSC metal-ion PSE was achieved with isostructural Pb<sup>II</sup> and Cd<sup>II</sup> MOFs by placing the Cd<sup>II</sup>-based framework in an aqueous solution of Pb(NO<sub>3</sub>)<sub>2</sub>.<sup>[197]</sup> The process was reversible, with Cd<sup>II</sup> being able to displace Pb<sup>II</sup> from the MOF. The Cd<sup>II</sup> ions could also be replaced by Dy<sup>III</sup> or Nd<sup>III</sup> ions, despite the difference in charge, demonstrating the power of PSE to produce frameworks that could not be accessed by direct synthesis. Subsequent studies on metal-ion PSE using metals that produced different colors provided insight into the PSE process and synthetic access to heterometallic core-shell MOF structures.<sup>[217]</sup> Metal-ion PSE studies require careful characterization of the MOF products. Indeed, even with substantial characterization, the author of this section once misidentified a metal-ion PSE process in a series of UiO-type MOFs; what was originally described as PSE of Zr<sup>IV</sup> for metal ions such as Ti<sup>IV</sup> or Hf<sup>IV</sup>,<sup>[218]</sup> was later identified as the formation of a thin metal oxide coating on the surface of the MOF crystallites.<sup>[219]</sup>

With respect to ligand PSE in MOFs, one early study showed that the pillaring ligands in the paddlewheel MOF PPF-18 could be exchanged.<sup>[198]</sup> Specifically, the “parent” MOF was prepared with the long pillaring linker *N,N*-di-4-pyridyl-naphthalenetetracarboxydiimide (DPNI). Soaking PPF-18 in a DEF/ethanol solution of 4,4'-bipyridine resulted in pillaring ligand PSE, producing a “daughter” framework (PPF-27) in a SCSC fashion. The approach was shown to be general with a structurally distinct MOF, PPF-20, which upon incubation with 4,4'-bipyridine was transformed via PSE into the isoreticular PPF-4.<sup>[198]</sup> This approach can also be applied

for the introduction of longer ligands,<sup>[220]</sup> the creation of hierarchical structures,<sup>[221]</sup> and the introduction of functionalized ligands.<sup>[222]</sup>

#### 9.4. Progress in PSM

Since the early findings on PSM, PSD, and PSE, the field has expanded dramatically and more complex transformations, including multiple tandem or serial PSM reactions, as well as complex combinations of PSM and other postsynthetic methods (e.g., PSD, PSE) have been reported.

Zr<sup>IV</sup> or Hf<sup>IV</sup> frameworks (of the UiO type) constructed from 4,4'-ethynylendibenzoate ligands undergo PSM with Br<sub>2</sub> in a stereoselective manner.<sup>[223]</sup> SCRXD of the brominated PSM MOF showed a 3.7% reduction in unit cell volume due to a change in the hybridization of the carbon atoms in the MOF linkers, highlighting that PSM can be used to alter both the chemical and structural features of a MOF.<sup>[224]</sup>

Spray drying can be used to perform imine condensations on amine- or aldehyde-tagged MOFs in a matter of seconds, thereby significantly reducing reaction times and thus making PSM suitable for coatings, films, and related industrial processes.<sup>[200]</sup> Spray drying an ethanol solution of UiO-66-NH<sub>2</sub><sup>[225]</sup> with a variety of aromatic aldehydes instantaneously produced MOF powders with up to 20% conversion. Similarly, spray drying of ZIF-90<sup>[211]</sup> in the presence of various amines resulted in up to 42% conversion to the imine products.<sup>[200]</sup> Solid MOF crystals can be treated with a gaseous reagent to effect the PSM reaction. Using a stream of ozone, pendant alkene groups in UiO-66 were quantitatively transformed into 1,2,4-trioxolane groups by ozonolysis in a SCSC manner.<sup>[201]</sup> Depending on the workup conditions, one of two final products could be produced from the resulting trioxolane MOF (pendant aldehyde or carboxylic acid). Such alternative reaction conditions (solid and gas phase) may overcome many of the limitations of conventional solid/solution phase PSM chemistry.

Beyond new organic reactions, the use of PSM to make new materials has seen continuous growth and led to exciting results. Using a variety of multifunctional linkers and multifunctional reagents, PSM has been used to connect multiple ligands together, ultimately stitching the MOF into a three-dimensional monolithic gel.<sup>[226,227]</sup> Some of these reports have shown that the resulting MOF gels are sufficiently crosslinked such that the soft gels retain the facets and edges of the parent MOF crystals, even upon swelling in solvent. In addition, by clever selection of the MOF, crosslinker, and PSM reaction, MOF-derived gels have been produced that display anisotropic swelling, a feature reminiscent of muscle tissue and other biological structures.<sup>[227,228]</sup>

## 10. MOF Nanoparticles

As established in the previous sections, MOFs present a unique variety of structures and properties that can be tailored through rational design. Size is an interesting

addition to the variables that contribute to determining the features of a material. Usually, MOFs are investigated at the macroscopic level in bulk assemblies with crystal domains that are significantly varied in size. Moving to the nanoscopic size, new properties arise—high surface-to-volume ratio and the possibility to make colloidal suspensions that bridge the boundaries between solids and molecules.<sup>[229–232]</sup> The rationalization of MOF nanoparticle chemistry has provided and keeps providing key insights into reticular chemistry, in particular with regard to nucleation and growth processes.

There are three main factors to control MOF nanoparticles in order to achieve monodisperse size distributions and morphologies: nucleation, crystal growth and agglomeration processes. To study and rationalize the first two processes, the LaMer model is an unparalleled tool.<sup>[233]</sup> This model divides the growth of the NPs into three different stages: 1) precursors dissolve until supersaturation is achieved, followed by the formation of reactive species; 2) when the critical concentration of reactive monomers is reached, nucleation takes place; 3) when nucleation occurs, the concentration of reactive monomers decreases, halting the nucleation process; crystal growth then starts and continues until an equilibrium is reached. Thus, to achieve nanoparticles with uniform size, a very short nucleation period must be achieved, while to obtain nanoparticles with the desired dimensions, the key factor is the growth time of each nucleus.<sup>[234]</sup>

Solvothermal synthesis is especially important for MOFs that require synthetic conditions not possible with other techniques (i.e. high pressure). Synthetic parameters such as concentration, temperature, pressure, and stirring speed can be easily changed while refining the synthesis of the desired particles. Compared to “traditional” solvothermal MOF synthesis, shorter reaction times and different dilutions lead to nanocrystals instead of micro- or macrocrystals.<sup>[235]</sup> Microwave-assisted synthesis differs from classic solvothermal synthesis in the fact that microwave heating is faster than conventional heating.<sup>[236]</sup> This improved heating leads to up to 30 times faster nucleation and growth of the nanoparticles, improving their homogeneity in morphology and shape.<sup>[237]</sup> Syntheses within less than 10 seconds have been reported with this technique.<sup>[238]</sup> Another useful heating source that accelerates particle nucleation is ultrasound irradiation. In this case, heat is not applied homogeneously, but ultrasonic waves cause cavitation bubbles in the solution, generating points of extreme heat and pressure in the solution when the bubbles collapse. These points of extreme heat and pressure start the nucleation and permit the growth of the nanoparticles.<sup>[239]</sup> Although extremely fast, this technique leads to particles with poor morphology, and difficulty in control over their size. A kinetic study of these three different methods demonstrated that ultrasonication is two orders of magnitude faster than solvothermal synthesis and one order of magnitude faster than microwave-assisted synthesis.<sup>[240]</sup>

Microfluidic flow reactors follow a different, non-bulk, approach, as the precursor solutions are mixed and forced in sub-millimetric channels. Due to the small channel size, heating is extremely effective and localized, and its application can be controlled to within a fraction of a second by

simply varying the flow rate of the solution through the apparatus. Varying the length of the tube and the flow rate of the solutions allows for an excellent control over the mixing time, and thus nanoparticle size and morphology, as well as for very fast reaction speed.<sup>[241,242]</sup> Micro-confinement is also used in reverse-phase microemulsion reactions, where the macro- and the microscales combine. Here, instead of solutions in solvothermal setups, micro- or nanodroplets of polar solvents are stabilized by surfactants emulsified in an oil bath. This synthetic technique achieves nanosized reactors in which only few nanoparticles can grow at the same time, ensuring good uniformity in the emulsion, but favoring aggregation, especially at high reactant concentrations.<sup>[243]</sup> If this approach is taken to its limit, it can produce interesting spherical microaggregates of nanoparticles.<sup>[244]</sup>

Once synthesized, a material must be characterized, and the reproducibility of the synthetic procedure must be thoroughly checked. Characterizing nanoparticles is not trivial, but the sensible use of different techniques can form a detailed picture of their properties.<sup>[245,246]</sup>

The crystal surface is a key feature of a nanoparticle, as it determines its behavior in the suspension medium. If the surface has more affinity toward itself than the medium, the particles will aggregate. This process leads to polycrystalline particles with a broader size dispersion and varied morphology and results, ultimately, in their precipitation from the suspension.<sup>[247]</sup> For this reason, surface functionalization has become crucial in determining the desired behavior of the particles and their interaction with the surroundings. The surface of a MOF present two kind of sites useful for functionalization: partially uncoordinated metal centers and organic linkers. It has been demonstrated that it is possible to form coordination bonds between the surface-exposed metal centers of a MOF and the functionalizing molecule, achieving complete surface functionalization under mild reaction conditions.<sup>[248]</sup> More common is the functionalization of MOF nanoparticles through covalent bonds by either reacting the uncoordinated bonding sites of the linkers exposed on the surface or reacting secondary functional groups present on the MOF's organic linker.<sup>[249,250]</sup> This approach has been proven successful in functionalizing various MOF nanoparticle with natural macromolecules, such as peptides and DNA strands.<sup>[249,251]</sup> Recently, it has been demonstrated that nanoparticles functionalized with compatible DNA strands can form superlattice assemblies.<sup>[252]</sup> These assemblies are ordered 3D superstructures formed by the periodic stacking of nanoparticles with uniform morphology. These bulk materials are held together by weak interactions and present interesting properties of photonic crystals, depending on the size of the constituent particles.<sup>[253,254]</sup>

The study of MOF nanoparticles is constantly expanding and leading to a better understanding of the whole field of reticular materials (Figure 9). The application of rigorous and standardized characterization protocols will provide common ground for the rationalization of the field. A deeper understanding of the synthesis and properties of MOF nanoparticles will extend their possible application to new and uncharted fields.

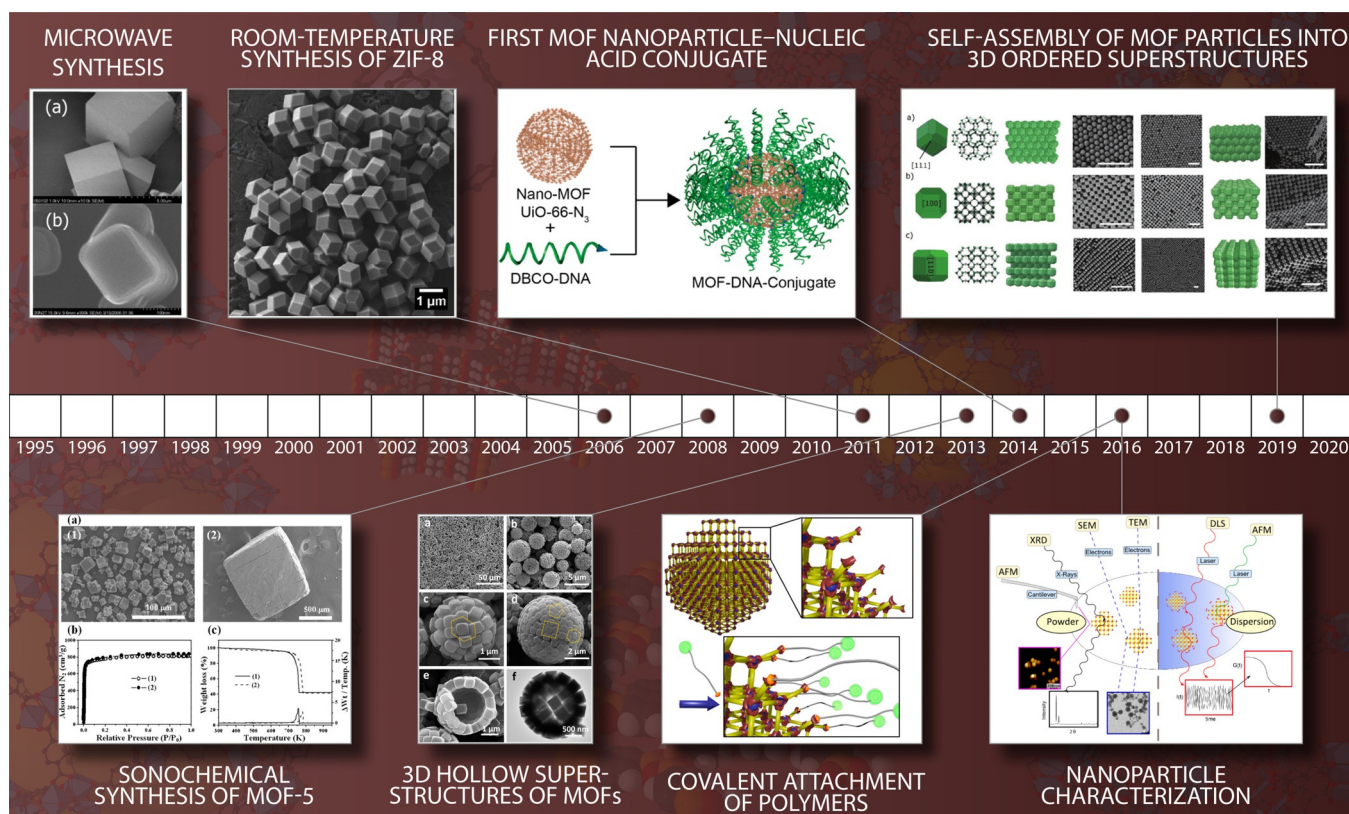


**Figure 9.** Illustrative timeline of the milestones in MOF nanoparticles. Microwave synthesis (reproduced with permission from ref. [236], Copyright 2006 American Chemical Society). Sonochemical synthesis of MOF-5 (reproduced with permission from ref. [239], Copyright 2008 The Royal Society of Chemistry). Room-temperature synthesis of ZIF-8 (reproduced with permission from ref. [234], Copyright 2011 American Chemical Society). 3D hollow superstructures of MOFs (reproduced with permission from ref. [244], Copyright 2013 American Chemical Society). First MOF nanoparticle-nucleic acid conjugate (reproduced with permission from ref. [249], Copyright 2014 American Chemical Society). Covalent attachment of polymers (reproduced with permission from ref. [250], Copyright 2016 American Chemical Society). Nanoparticle characterization (reproduced with permission from ref. [246], Copyright 2016 The Royal Society of Chemistry). Self-assembly of MOF particles into 3D ordered superstructures (reproduced with permission from ref. [253], Copyright 2019 Wiley-VCH).

## 11. Reticular Thin Films

While most of the reported synthesis routes for reticular materials yield powdery products, many of their numerous applications require their isolation as thin films (e.g., for optical applications, devices involving charge transport, and for the fabrication of membranes).<sup>[255]</sup> Key parameters determining the functionality and performance of such systems are lateral film dimensions, crystallographic orientation, thickness, homogeneity, roughness, crystallite orientation, defect concentration, and absence of pinholes.<sup>[256]</sup> These requirements have led to the development of a large number of different thin-film synthesis methods (Figure 10), opening up a vast parameter space for the optimization of these properties with regard to an ever increasing number of applications.<sup>[257,258]</sup>

### 11.1. Synthesis Methods

One of the most obvious routes to reticular thin films is to deposit particles fabricated by conventional methods on a solid support.<sup>[259–262]</sup> Alternatively, nonconventional syn-

thesis schemes allow the direct growth of such films on appropriately modified substrates (e.g., via formation of self-assembled monolayers).<sup>[263]</sup> This type of direct synthesis can be realized either by heterogeneous nucleation on a substrate<sup>[264]</sup> or by using layer-by-layer methods where the reactants are kept apart.<sup>[265]</sup> In addition, chemical vapor deposition schemes have been reported, for example by using coordinative replication of metal oxide thin films by chemical vapor deposition.<sup>[266]</sup> The synthesis parameters can be fine-tuned to adjust thickness and control surface roughness,<sup>[267]</sup> as well as to control the crystallographic orientation of the deposited film.<sup>[268]</sup> Also the realization of heterolayers using (quasi) epitaxy becomes possible,<sup>[256,269]</sup> introducing the possibility for integration concentration gradients. A straightforward way to achieve preferential orientation specific to COFs is to invoke  $\pi$ - $\pi$  interactions between flat aromatic building blocks and graphene-based substrates.<sup>[268]</sup> Instead of directly nucleating and growing the entire reticular thin film from the mother solution, it is possible to control the thin-film thickness by supplying the precursors in an alternating fashion. Numerous variants of such layer-by-layer methods have been reported,<sup>[265]</sup> resulting in the realization of a number of casting methods.<sup>[273]</sup> Another approach is so-called vapor-assisted

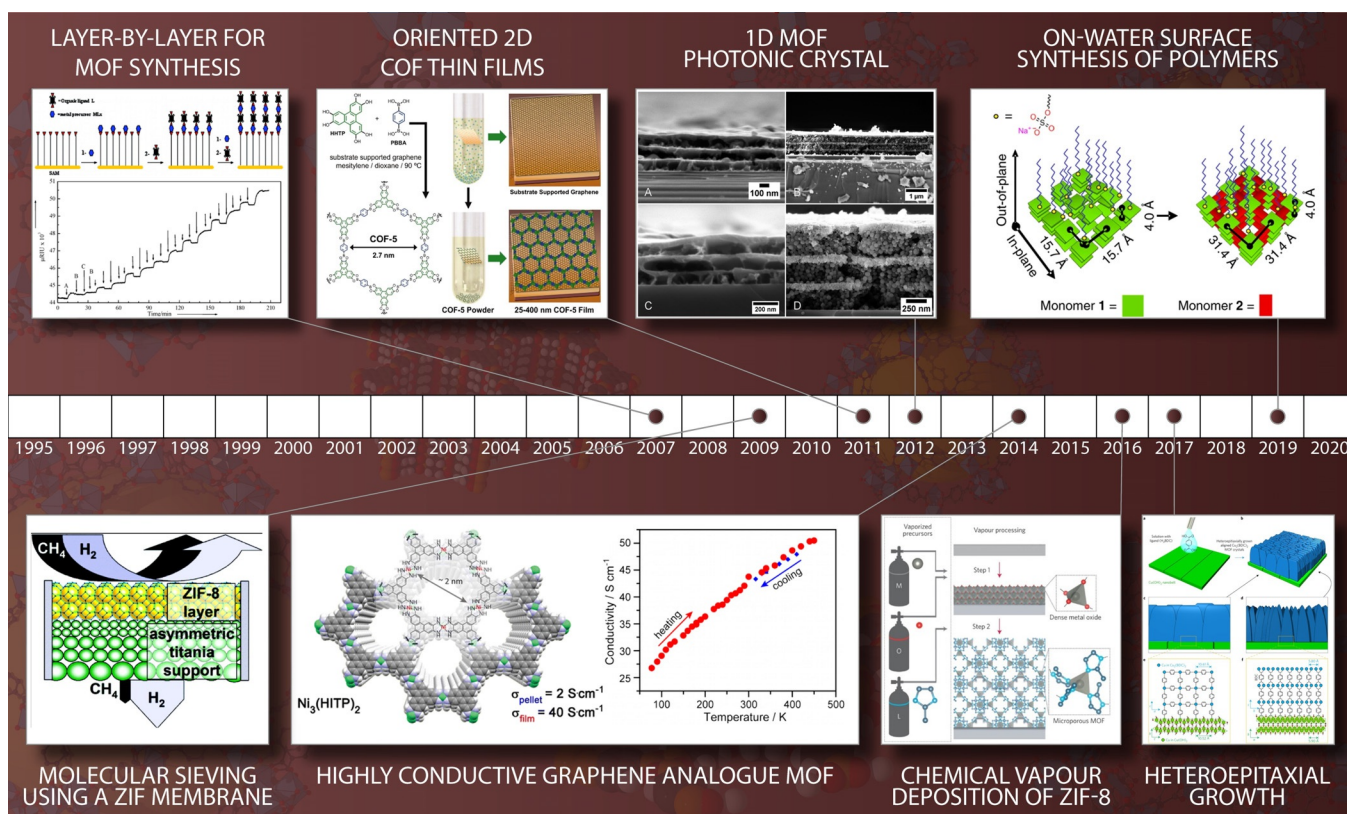


**Figure 10.** Illustrative timeline of the milestones in reticular thin films. Layer-by-layer for MOF synthesis (reproduced with permission from ref. [265], Copyright 2007 American Chemical Society). Molecular sieving using a ZIF membrane (reproduced with permission from ref. [270], Copyright 2009 American Chemical Society). Oriented 2D COF films (reproduced with permission from ref. [268], Copyright 2011 American Association for the Advancement of Science). 1D MOF photonic crystal (reproduced with permission from ref. [264], Copyright 2012 Royal Society of Chemistry). Highly conductive graphene analogue MOF (reproduced with permission from ref. [271], Copyright 2014 American Chemical Society). Chemical vapor deposition of ZIF-8 (reproduced with permission from ref. [266], Copyright 2016 Springer Nature). Heteroepitaxial growth (reproduced with permission from ref. [256], Copyright 2017 Springer Nature). On-water surface synthesis of polymers (reproduced with permission from ref. [272], Copyright 2019 Springer Nature).

conversion, where first a precursor thin film is deposited, which is then converted into a reticular thin film by exposure to solvent vapors.<sup>[274,275]</sup> Interfacial growth in biphasic systems allows the fabrication of self-supported thin films at the air/solvent<sup>[276]</sup> or solvent/solvent interface.<sup>[277]</sup> The latter approach can also be used to first orient precursors, which are then converted into a COF while maintaining the original orientation.<sup>[272]</sup> The Langmuir–Blodgett method allows the formation of molecular monolayers, which can then be transferred onto solid substrates.<sup>[278]</sup>

## 12. MOFs at the Mesoscopic and Macroscopic Scale

Reticular chemistry endows MOFs and COFs with tremendous opportunities to tune the properties at the molecular level. For practical applications, further assembling and shaping of these materials into desired meso-architectures and bulk physical forms are of great significance.<sup>[19,257]</sup> Modulating the shape of MOFs and COFs at the bulk scale to meet the requirements in application scenarios is vital for the optimal performance of these materials. In this section, the shaping strategies used to generate reticular materials with

diverse superstructures and distinctive morphologies will be summarized (Figures 11 and 12).

### 12.1. Reticular Meso-Superstructures

Reticular superstructures can be evolved based on Ostwald ripening,<sup>[279]</sup> surface-energy-driven<sup>[280]</sup> and self-templating<sup>[281]</sup> mechanisms, and the key is finding the appropriate conditions for intermediates. In the self-templating mechanism, intermediates forming in the early stage act as the self-template for the second growth and evolve into particular structures. In one case of COF hollow spheres, crystallites first assembled into spheres that further developed into hollow superstructures due to inside-out Ostwald ripening.<sup>[282]</sup> Modulators or competitors can be used to control the crystal growth, ultimately achieving the manipulation of the micro-/macroscale morphology. In this way, COFs with different morphologies, including spheres, fibers, and films were obtained due to the enhanced reversibility of the reaction.<sup>[296]</sup> Selectively etching the core parts of the structures may lead to hollow architectures. Polyphenolic acid was employed as an etching agent to engineer voids in MOFs, and its synergistic

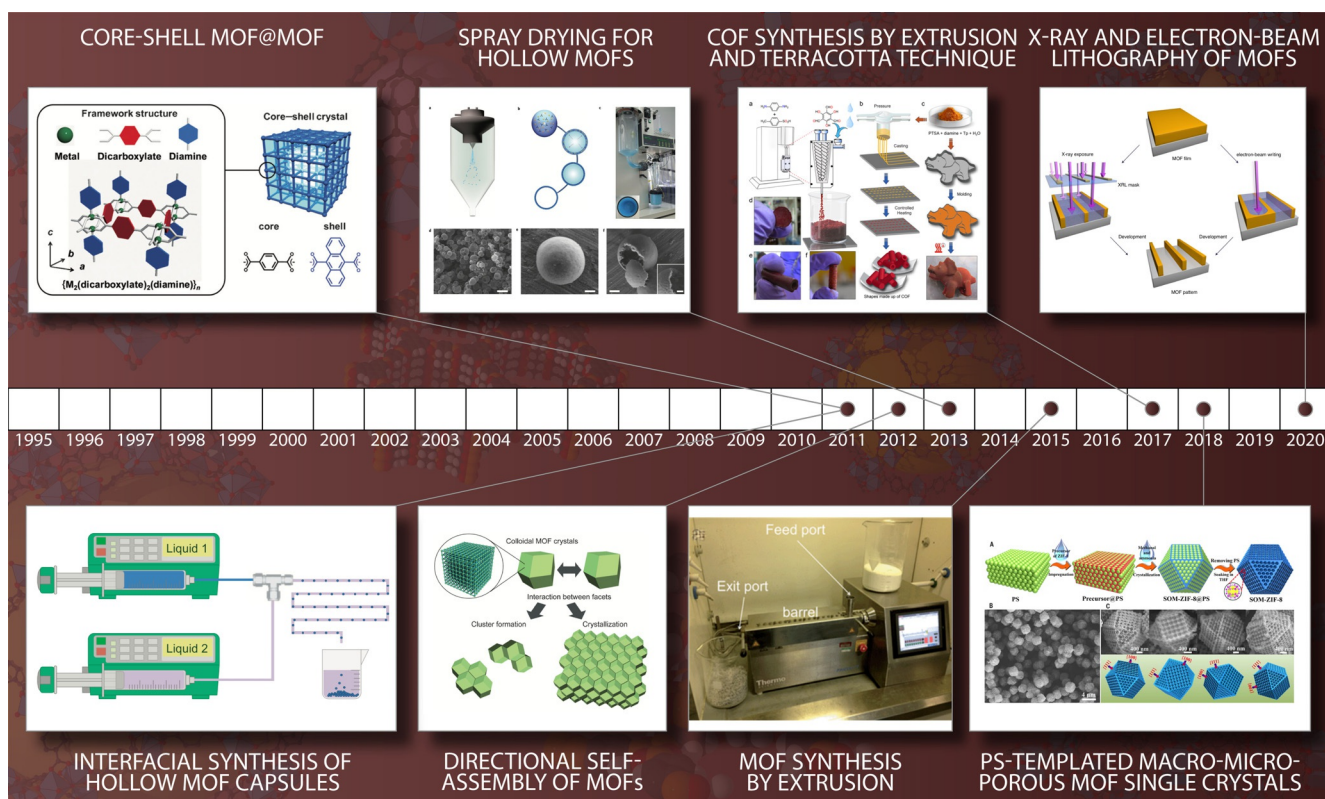


**Figure 11.** Illustrative timeline of the milestones in the shaping of reticular materials at the meso and bulk scale. Core-shell MOF@MOF (reproduced with permission from ref. [283], Copyright 2011 Wiley-VCH). Interfacial synthesis of hollow MOF capsules (reproduced with permission from ref. [284], Copyright 2011 Springer Nature). Directional self-assembly of MOFs (reproduced with permission from ref. [285], Copyright 2012 Wiley-VCH). Spray drying for hollow MOFs (reproduced with permission from ref. [286], Copyright 2013 Springer Nature). MOF synthesis by extrusion (reproduced with permission from ref. [287], Copyright 2015 The Royal Society of Chemistry). COF synthesis by extrusion and terracotta technique (reproduced with permission from ref. [288], Copyright 2017 American Chemical Society). PS-templated macro-microporous MOF single crystals (reproduced with permission from ref. [289], Copyright 2018 American Association for the Advancement of Science). X-ray and electron-beam lithography of MOFs. (reproduced with permission from ref. [290], Copyright 2020 Springer Nature).

surface function protects the frameworks from full destruction.<sup>[297]</sup> X-ray and electron-beam lithography of MOFs was conducted, affording high-quality patterns with resolution of sub-50 nm.<sup>[290]</sup> Sophisticated forms including single- and double-shell hollow MOFs were fabricated by a sequential self-assembly strategy that is based on the metal-organic polyhedral (MOP)-to-MOF conversion, in which the MOP core was chemically etched.<sup>[298]</sup>

For preformed uniform reticular nanocrystals, well-organized assembly can be realized through interparticle interactions and/or external driving forces. For example, capillary forces or van der Waals attractions can induce the spontaneous assembly of MOF nanoparticles, affording self-assembled clusters as well as ordered 3D superstructures.<sup>[285]</sup> An external electric field was employed to guide the particle assembly forming linear chains, and induced dipolar attractions between ZIF-8 crystals were responsible for the attachment.<sup>[299]</sup> To enhance the interactions between particles, polymer chains and covalent bonds were introduced to assist the construction of MOF and COF monolayers. Specifically, ZIF-8 nanoparticles covalently coated with a layer of polymer were self-assembled on a liquid-air interface as the polymer shell fused.<sup>[300]</sup> In the covalent self-assembly approach, the residual functionality on the surface

of COF nanospheres promotes the covalent bonding by dynamic covalent chemistry.<sup>[301]</sup>

Spatial control of the reaction systems and precise manipulation of the assembly can be realized by employing hard or soft templates that can induce the nucleation and crystal growth on the preshaped surfaces. The main advantage of this method lies in the direct and facile modulation of the superstructures' shapes. In addition, the templates may also introduce special features, resulting in composite superstructures with enhanced and versatile functions.

Hard templates for the construction of reticular mesostructures include polymers, metal oxides, and inorganic salts, and their rigid structure can directly influence the morphology of the products. Polystyrene (PS) nanospheres are effective templates for shaping, and in situ growth of ZIF-8 within the voids of the PS monolith templates successfully led to single crystals with ordered macro-micropores.<sup>[289]</sup> Shaped metal oxides can serve as metal sources as well as structure-directing agents, which could offer more available configurations for replication due to their well-established morphology control procedures. In a coordination replication strategy, local dissolution of the alumina template and crystallization of Al-MOF on the interface ensured the preservation of the parent structure.<sup>[302]</sup> MOF hollow super-

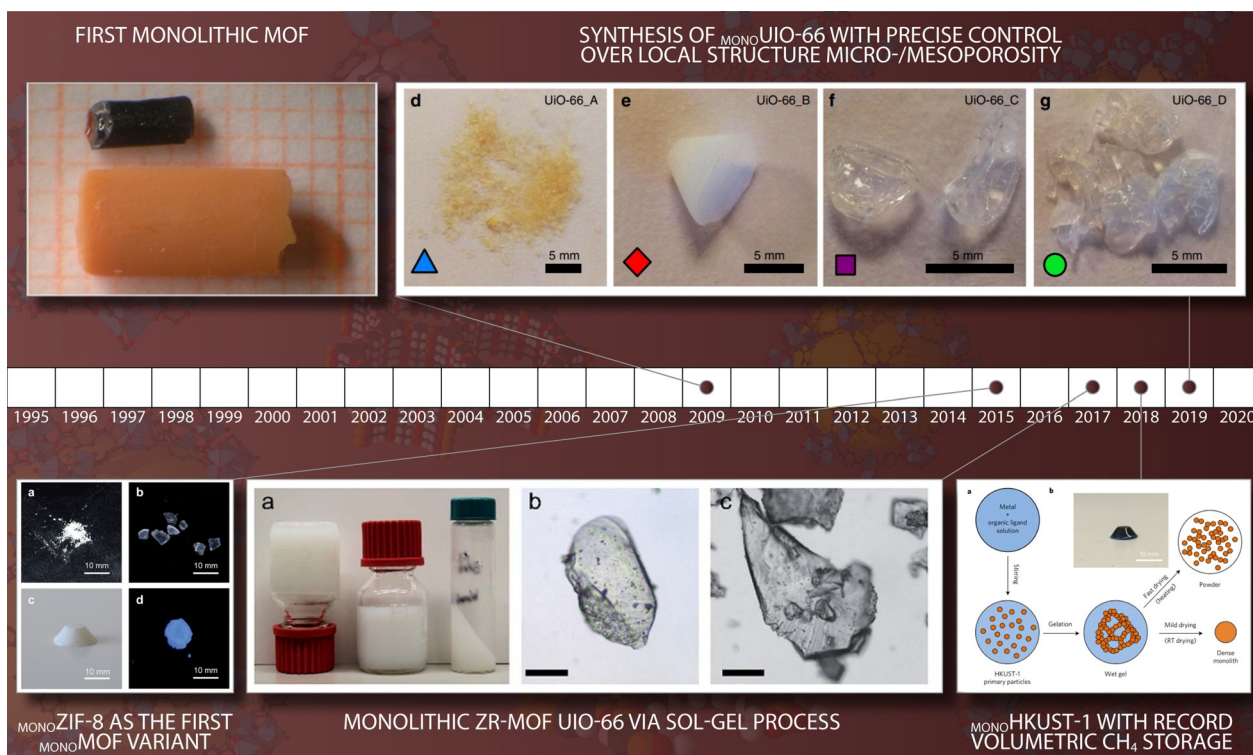


**Figure 12.** Illustrative timeline of the milestones in monolithic reticular materials. First monolithic MOF (reproduced with permission from ref. [291], Copyright 2009 The Royal Society of Chemistry). MONOZIF-8 as the first MONOMOF variant (reproduced with permission from ref. [292], Copyright 2015 The Royal Society of Chemistry). Monolithic Zr-MOF UiO-66 via sol-gel process (reproduced with permission from ref. [293], Copyright 2017 The Royal Society of Chemistry). MONOHKUST-1 with record volumetric  $\text{CH}_4$  storage (reproduced with permission from ref. [294], Copyright 2018 Springer Nature). Synthesis of MONOUIO-66 with precise control over local structure and micro-/mesoporosity (reproduced with permission from ref. [295], Copyright Springer Nature 2019).

structures could be evolved from metal salts and metal oxide as a result of diffusion effects.<sup>[303]</sup> Similarly, MOPs and MOFs can also be used as the sacrificial templates, and hollow single-crystalline and box superstructure MOFs<sup>[304]</sup> were successfully fabricated.

Functional templates can be introduced to further increase composition and structure complexity. Templated by  $\text{Fe}_3\text{O}_4$  nanoclusters, core-shell COF microspheres with magnetic responsiveness were prepared by an amorphous-to-crystalline transformation strategy.<sup>[305]</sup> Core-shell structures can be applied for structuring yolk-shell or capsule composites, where the selective decomposition of the inner shell results in a cavity in between them.<sup>[306]</sup> In this way, nanocrystals and biomolecules were included in reticular porous shells with fully exposed surfaces. Specially, the controlled growth of reticular frameworks can also be directed by another reticular component core giving structured MOF@MOF, MOF@COF, and COF@COF.<sup>[283,307,308]</sup>

Soft template methods generally utilize the micelles or aggregates formed by intramolecular or intermolecular interactions, featuring tunable structures and facile removal. Surfactants are mostly employed since they can form supramolecular assemblies with tunable morphologies and nucleation sites. An example is the construction of helical MOF nanotubes, in which amphiphilic templates form helical supramolecular aggregates and induce the growth of MOFs

on the surface.<sup>[309]</sup> Determined by the packing forms of the surfactants, MOFs with hollow sphere and ring-like structures were also achieved. Specially, cell walls themselves are hollow structures with porous walls, and can be used for inside/outside interfacial crystallization of continuous MOF layers, giving MOF/cell wall microcapsules with size selectivity.<sup>[310]</sup>

Liquid-liquid and gas-liquid interfaces can be considered as special soft templates, offering confined spaces for precise localization and controlled construction of superstructures, which have been applied for nanosheet and film preparation. When molded membranes or micropatterned substrates were introduced, MOF superstructure patterns with defined shape could be engineered.<sup>[311]</sup> Droplets are effective spherical templates for the fabrication of hollow structures, which can be formed in the emulsion system,<sup>[244]</sup> microfluidic environment,<sup>[284]</sup> and spray-drying process.<sup>[286]</sup>

## 12.2. Reticular Framework Monoliths

While MOFs have shown potential for use in a wide range of applications, their use in industrial processes has been limited by a lack of practical options for materials shaping.<sup>[19]</sup> The shaping of MOF powders into bulk samples with desired size, shape, density, and mechanical stability is a critical step for their industrial deployment.<sup>[312]</sup> Mechanical shaping is the

most common method for forming shaped bodies from powders and can be divided into several subclasses, including granulation, extrusion, and pressing.<sup>[313]</sup> Mechanical shaping has already been widely utilized for shaping MOFs, including prototypical materials such as HKUST-1,<sup>[287]</sup> ZIF-8,<sup>[314]</sup> UiO-66,<sup>[315]</sup> and Ni-MOF-74<sup>[316]</sup> (Figure 11). While mechanical shaping is relatively simple and fast, the resulting materials often display two major issues. On one hand, extruded materials where low mechanical pressures are applied can often display low bulk densities due to the presence of large void spaces as a result of the use of low mechanical pressure or the removal of binder during the aging step. Conversely, in powder pressing, the delicate crystalline structures of MOFs are prone to collapse under high mechanical pressures, leading to crumple zones of amorphous material.<sup>[317]</sup> These amorphous phases can give way to pellets with high bulk densities but with large reductions in the overall porosity. In some cases, pressing may present positive effects such as enhanced mechanical strength and catalytic activity. It was also observed that the pressed COF pellets show anisotropic ordering with preferred orientation.<sup>[318]</sup> As for granulation and extrusion, wet technology techniques are generally applied as the binders and/or solvents would enhance the processability and mechanical strength of the shaped materials, despite the potential of porosity loss. Inorganic binders such as alumina, silica, siloxane, and kaolin have been utilized for shaping, and organic binders such as cellulose, methyl cellulose, alginate, and polyvinyl alcohol are commonly used. Uniform spheres or beads can be acquired using granulators, syringes, and centrifuges. With the assistance of a screw or plunger, shaped bodies can be produced continuously with high efficiency; promisingly, single- and twin-screw extruders have been successfully applied for the continuous synthesis of MOFs<sup>[287]</sup> and COFs,<sup>[288]</sup> with potential for scaled-up production.

In contrast to traditional shaping, self-shaping methods can effectively circumvent the issues related to extrusion and high-pressure pressing of MOF shaped bodies. Self-shaping can eliminate the need for additives and/or use of mechanical presses or extruders. This unique methodology holds promise for reducing performance-related issues for MOF shaping whilst simultaneously reducing the cost for the production of shaped MOF materials.

So far, there have only been a limited number of reports on self-shaping MOFs. One of the first MOFs found to be capable of self-shaping was Fe-BTC.<sup>[291]</sup> In this study, researchers found that the precursor MOF gels would form powders with heat-aided drying, while self-shaped materials formed via syneresis when the MOF gel was dried at room temperature. The shaped Fe-BTC sample was found to be hierarchically porous, containing ca. 8 times more porosity than the powdered Fe-BTC xerogel dried at elevated temperature.

The importance of this study went relatively unnoticed until the recent development of monolithic MOFs (*mono*-MOFs). Similar to previously reported monolithic gels, monolithic MOFs are formed via a sol-gel synthesis approach, offering a viable alternative to traditional MOF shaping processes. *mono*-MOFs enable the synthesis of high-

density, mechanically and chemically stable, centimeter-scale shaped materials, which retain their porosity during synthesis. The first such report on monolithic MOF synthesis came with the development of *mono*-ZIF-8.<sup>[292]</sup> The transparent, glassy-looking material displayed high bulk mechanical strength (hardness,  $H$ , = 0.43 GPa) and BET area ( $S_{\text{BET}} = 1423 \text{ m}^2 \text{ g}^{-1}$ ) and a density of  $r_b = 1.05 \text{ g cm}^{-3}$  (crystal  $r_b = 0.95 \text{ g cm}^{-3}$ ). This methodology was subsequently modified to encapsulate  $\text{SnO}_2$  nanoparticles to form  $\text{SnO}_2@_{\text{mono}}\text{ZIF-8}$ ,<sup>[319]</sup> a catalytically active variant of *mono*-ZIF-8 capable of degrading aqueous methylene blue via photocatalysis. The *mono*-ZIF-8 synthesis was further modified in a recent study to form MAF-4 monoliths via ligand substitution.<sup>[320]</sup> The MAF-4/ZIF-8 composite monoliths were found to display high optical transmittance (69% to 84%) in the visible light region (400 to 700 nm).

This sol-gel synthesis approach was subsequently extended to other MOFs, starting with HKUST-1.<sup>[294]</sup> The remarkable physical and mechanical properties displayed by *mono*-HKUST-1 ( $r_b = 1.06 \text{ g cm}^{-3}$ ,  $S_{\text{BET}} = 1288 \text{ m}^2 \text{ g}^{-1}$ , and  $H = 0.46 \text{ GPa}$ ) resulted in an outstanding volumetric methane uptake capacity of  $261 \text{ cm}^3 \text{ (STP) cm}^{-3}$  (65 bar, 298 K). This was found to substantially exceed the previously reported results for pelletized HKUST-1 compacted under a range of pressures; in the case of *mono*-HKUST-1, the higher density of the monolith did not have a detrimental impact on its porosity.<sup>[321]</sup> The benchmark volumetric methane uptake of the densified *mono*-HKUST-1 rendered it the first material to effectively reach the DOE target for methane storage.<sup>[322]</sup>

Issues regarding the stability of HKUST-1 prompted researchers to pursue *mono*-MOF variants from families of stable MOF materials. Through a gel-based synthesis, different groups have extended the possibility of creating *mono*-MOFs to the highly stable UiO-66 family.<sup>[293]</sup> Initial studies produced UiO-66 materials with low densities (ca.  $0.39 \text{ g cm}^{-3}$ ) and large amounts of meso- and macroporosity. Recently, the formation of *mono*-UiO-66 was achieved by varying the sol-gel drying conditions employed during synthesis.<sup>[295]</sup> The bulk physical properties of *mono*-UiO-66 were tuned with a high level of experimental control, resulting in materials with bulk densities varying between 0.43 and  $1.05 \text{ g cm}^{-3}$  (crystal  $r_b = 1.20 \text{ g cm}^{-3}$ ). Fluorescence lifetime imaging microscopy (FLIM) of *mono*-UiO-66 revealed that the highly transparent materials consisted of primary particles which aggregated as a result of close physical proximity. The inclusion of mesoporosity and its resultant alteration to the adsorptive properties of the MOF yielded outstanding improvements in the methane working capacity of *mono*-UiO-66 ( $261 \text{ cm}^3 \text{ (STP) cm}^{-3}$ , 5–100 bar, 298 K). This study demonstrated that unprecedented levels of synthetic control can be exerted on local structures of *mono*-MOFs, enabling the enhancement of gas adsorption properties beyond theoretical maxima of purely microporous materials.

### 13. Outlook

Twenty-five years after the landmark discovery of the first MOF and the concomitant emergence of the field of reticular

chemistry the field has matured into a broad, multidisciplinary area of research. At the core of reticular chemistry is the design and synthesis of new materials starting from molecular building blocks, their reticulation into extended solids, and their postsynthetic modification. Over the past years, while the number of MOF and COF papers is constantly increasing, the yearly number of new entries in the CSD database has started decreasing. While the enthusiastic molecular architect will always identify new challenges in designing innovative MOFs structures, the trend nonetheless suggests that the field has reached a certain level of maturity with respect to material discovery and that the focus is now shifting toward other aspects of synthesis, as well as the design and identification of materials with specific properties. The latter aspect poses new challenges to understanding MOFs and COFs that go beyond information about the average structure and focuses more on phenomena such as complexity, multivariance, and disorder. For many of these challenges, reticular chemistry is uniquely suited to identify solutions that might benefit not only researchers in the field but of chemistry and material science as a whole. Finally, there is an increased effort to control reticular materials beyond the framework and the elaboration of techniques to control their morphology and shape from the nanoscale (nanocrystals and films) all the way to the bulk with monoliths and the shaping of these materials. We predict that the next 25 years will see an increased focus on the development of these areas of reticular chemistry.

### Conflict of Interest

The authors declare no conflict of interest.

- [1] O. M. Yaghi, M. O'Keeffe, N. W. Ockwig, H. K. Chae, M. Eddaoudi, J. Kim, *Nature* **2003**, *423*, 705–714.
- [2] H. Li, M. Eddaoudi, T. L. Groy, O. M. Yaghi, *J. Am. Chem. Soc.* **1998**, *120*, 8571–8572.
- [3] H. Li, M. Eddaoudi, M. O'Keeffe, O. M. Yaghi, *Nature* **1999**, *402*, 276–279.
- [4] Y. Kinoshita, I. Matsubara, Y. Saito, *Bull. Chem. Soc. Jpn.* **1959**, *32*, 1221–1226.
- [5] M. Fujita, J. Yazaki, K. Ogura, *J. Am. Chem. Soc.* **1990**, *112*, 5645–5647.
- [6] T. Beissel, R. E. Powers, K. N. Raymond, *Angew. Chem. Int. Ed. Engl.* **1996**, *35*, 1084–1086; *Angew. Chem.* **1996**, *108*, 1166–1168.
- [7] H. Furukawa, K. E. Cordova, M. O. Keffe, O. M. Yaghi, *Science* **2013**, *341*, 1230444.
- [8] C. Gropp, S. Canossa, S. Wuttke, F. Gándara, Q. Li, O. M. Yaghi, *ACS Cent. Sci.* **2020**, *6*, 1255–1273.
- [9] S. Kitagawa, R. Kitaura, S. I. Noro, *Angew. Chem. Int. Ed.* **2004**, *43*, 2334–2375; *Angew. Chem.* **2004**, *116*, 2388–2430.
- [10] G. Férey, *Chem. Soc. Rev.* **2008**, *37*, 191–214.
- [11] A. G. Slater, A. I. Cooper, *Science* **2015**, *348*, aaa8075.
- [12] O. M. Yaghi, M. J. Kalmutzki, C. S. Diercks, *Introduction to Reticular Chemistry: Metal-Organic Frameworks and Covalent Organic Frameworks*, Wiley-VCH, Weinheim, **2019**.
- [13] D. Ongari, L. Talirz, B. Smit, *ACS Cent. Sci.* **2020**, *6*, 1890–1900.
- [14] C. S. Diercks, O. M. Yaghi, *Science* **2017**, *355*, eaal1585.
- [15] A. P. Côté, A. I. Benin, N. W. Ockwig, M. O'Keeffe, A. J. Matzger, O. M. Yaghi, *Science* **2005**, *310*, 1166–1170.
- [16] H. M. El-Kaderi, J. R. Hunt, J. L. Mendoza-Cortés, A. P. Côté, R. E. Taylor, M. O'Keeffe, O. M. Yaghi, *Science* **2007**, *316*, 268–272.
- [17] A. F. Wells, *Acta Crystallogr.* **1965**, *18*, 894–900.
- [18] A. F. Wells, *Structural Inorganic Chemistry*, Oxford University Press, Oxford, **1985**.
- [19] F. Haase, P. Hirschle, R. Freund, S. Furukawa, Z. Ji, S. Wuttke, *Angew. Chem. Int. Ed.* **2020**, *59*, 22350–22370; *Angew. Chem.* **2020**, *132*, 22534–22556.
- [20] S. Subramanian, M. J. Zaworotko, *Angew. Chem. Int. Ed. Engl.* **1995**, *34*, 2127–2129; *Angew. Chem.* **1995**, *107*, 2295–2297.
- [21] G. Shimizu, R. Vaidyanathan, J. Taylor, *Chem. Soc. Rev.* **2009**, *38*, 1430–1449.
- [22] P. Tholen, Y. Zorlu, J. Beckmann, G. Yücesan, *Eur. J. Inorg. Chem.* **2020**, 1542–1554.
- [23] O. M. Yaghi, G. M. Li, H. L. Li, *Nature* **1995**, *378*, 703–706.
- [24] W. Mori, F. Inoue, K. Yoshida, H. Nakayama, S. Takamizawa, M. Kishita, *Chem. Lett.* **1997**, *26*, 1219–1220.
- [25] S. S. Y. Chui, S. M. F. Lo, J. P. H. Charmant, A. G. Orpen, I. D. Williams, *Science* **1999**, *283*, 1148–1150.
- [26] M. Kondo, T. Yoshitomi, K. Seki, H. Matsuzaka, S. Kitagawa, *Angew. Chem. Int. Ed. Engl.* **1997**, *36*, 1725–1727; *Angew. Chem.* **1997**, *109*, 1844–1846.
- [27] T. M. Reineke, M. Eddaoudi, M. Fehr, D. Kelley, O. M. Yaghi, *J. Am. Chem. Soc.* **1999**, *121*, 1651–1657.
- [28] M. Eddaoudi, J. Kim, N. Rosi, D. Vodak, J. Wachter, M. O'Keeffe, O. M. Yaghi, *Science* **2002**, *295*, 469–472.
- [29] J. H. Cavka, S. Jakobsen, U. Olsbye, N. Guillou, C. Lamberti, S. Bordiga, K. P. Lillerud, *J. Am. Chem. Soc.* **2008**, *130*, 13850–13851.
- [30] J. F. Eubank, F. Nouar, R. Luebke, A. J. Cairns, Ł. Wojtas, M. Alkordi, T. Bousquet, M. R. Hight, J. Eckert, J. P. Embs, et al., *Angew. Chem. Int. Ed.* **2012**, *51*, 10099–10103; *Angew. Chem.* **2012**, *124*, 10246–10250.
- [31] O. K. Farha, I. Eryazici, N. C. Jeong, B. G. Hauser, C. E. Wilmer, A. A. Sarjeant, R. Q. Snurr, S. T. Nguyen, A. Ö. Yazaydin, J. T. Hupp, *J. Am. Chem. Soc.* **2012**, *134*, 15016–15021.
- [32] V. Guillerme, D. Kim, J. F. Eubank, R. Luebke, X. Liu, K. Adil, M. S. Lah, M. Eddaoudi, *Chem. Soc. Rev.* **2014**, *43*, 6141–6172.
- [33] Y. Yan, S. Yang, A. J. Blake, M. Schröder, *Acc. Chem. Res.* **2014**, *47*, 296–307.
- [34] C. Serre, C. Mellot-Draznieks, S. Surblé, N. Audebrand, Y. Filinchuk, G. Férey, *Science* **2007**, *315*, 1828–1831.
- [35] Z. Chen, P. Li, R. Anderson, X. Wang, X. Zhang, L. Robison, L. R. Redfern, S. Moribe, T. Islamoglu, D. A. Gómez-Gualdrón, T. Yildirim, et al., *Science* **2020**, *368*, 297–303.
- [36] H. Furukawa, Y. B. Go, N. Ko, Y. K. Park, F. J. Uribe-Romo, J. Kim, M. O'Keeffe, O. M. Yaghi, *Inorg. Chem.* **2011**, *50*, 9147–9152.
- [37] J. F. Eubank, H. Mouttaki, A. J. Cairns, Y. Belmabkhout, Ł. Wojtas, R. Luebke, M. Alkordi, M. Eddaoudi, *J. Am. Chem. Soc.* **2011**, *133*, 14204–14207.
- [38] I. M. Hönicke, I. Senkovska, V. Bon, I. A. Baburin, N. Bönisch, S. Raschke, J. D. Evans, S. Kaskel, *Angew. Chem. Int. Ed.* **2018**, *57*, 13780–13783; *Angew. Chem.* **2018**, *130*, 13976–13979.
- [39] H. Deng, S. Grunler, K. E. Cordova, C. Valente, H. Furukawa, M. Hmadeh, F. Gándara, A. C. Whalley, Z. Liu, S. Asahina, et al., *Science* **2012**, *336*, 1018–1023.
- [40] M. O'Keeffe, O. M. Yaghi, *Chem. Rev.* **2012**, *112*, 675–702.
- [41] M. Li, D. Li, M. O'Keeffe, O. M. Yaghi, *Chem. Rev.* **2014**, *114*, 1343–1370.
- [42] Z. Chen, H. Jiang, M. Li, M. O'Keeffe, M. Eddaoudi, *Chem. Rev.* **2020**, *120*, 8039–8065.

- [43] O. Delgado-Friedrichs, M. O'Keeffe, O. M. Yaghi, *Acta Crystallogr. Sect. A* **2006**, *62*, 350–355.
- [44] M. Eddaoudi, J. Kim, M. O'Keeffe, O. M. Yaghi, *J. Am. Chem. Soc.* **2002**, *124*, 376–377.
- [45] H. Furukawa, J. Kim, N. W. Ockwig, M. O'Keeffe, O. M. Yaghi, *J. Am. Chem. Soc.* **2008**, *130*, 11650–11661.
- [46] V. Guillermin, T. Grancha, I. Imaz, J. Juanhuix, D. MasPOCH, *J. Am. Chem. Soc.* **2018**, *140*, 10153–10157.
- [47] V. Guillermin, D. MasPOCH, *J. Am. Chem. Soc.* **2019**, *141*, 16517–16538.
- [48] T. Devic, C. Serre, *Chem. Soc. Rev.* **2014**, *43*, 6097–6115.
- [49] G. Férey, C. Serre, C. Mellot-Draznieks, F. Millange, S. Surblé, J. Dutour, I. Margiolaki, *Angew. Chem. Int. Ed.* **2004**, *43*, 6296–6301; *Angew. Chem.* **2004**, *116*, 6456–6461.
- [50] G. Férey, C. Mellot-Draznieks, C. Serre, F. Millange, J. Dutour, S. Surblé, I. Margiolaki, *Science* **2005**, *309*, 2040–2042.
- [51] S. Horike, S. Shimomura, S. Kitagawa, *Nat. Chem.* **2009**, *1*, 695–704.
- [52] A. Schneemann, V. Bon, I. Schwedler, I. Senkovska, S. Kaskel, R. A. Fischer, *Chem. Soc. Rev.* **2014**, *43*, 6062–6096.
- [53] C. Serre, F. Millange, C. Thouvenot, M. Noguès, G. Marsolier, D. Louër, G. Férey, *J. Am. Chem. Soc.* **2002**, *124*, 13519–13526.
- [54] M. Dan-Hardi, C. Serre, T. Frot, L. Rozes, G. Maurin, C. Sanchez, G. Férey, *J. Am. Chem. Soc.* **2009**, *131*, 10857–10859.
- [55] D. Feng, Z. Y. Gu, J. R. Li, H. L. Jiang, Z. Wei, H. C. Zhou, *Angew. Chem. Int. Ed.* **2012**, *51*, 10307–10310; *Angew. Chem.* **2012**, *124*, 10453–10456.
- [56] H. Furukawa, F. Gándara, Y. B. Zhang, J. Jiang, W. L. Queen, M. R. Hudson, O. M. Yaghi, *J. Am. Chem. Soc.* **2014**, *136*, 4369–4381.
- [57] T. Tsuruoka, S. Furukawa, Y. Takashima, K. Yoshida, S. Isoda, S. Kitagawa, *Angew. Chem. Int. Ed.* **2009**, *48*, 4739–4743; *Angew. Chem.* **2009**, *121*, 4833–4837.
- [58] A. Schaate, P. Roy, A. Godt, J. Lippke, F. Waltz, M. Wiebcke, P. Behrens, *Chem. Eur. J.* **2011**, *17*, 6643–6651.
- [59] Z. Chen, S. L. Hanna, L. R. Redfern, D. Alezi, T. Islamoglu, O. K. Farha, *Coord. Chem. Rev.* **2019**, *386*, 32–49.
- [60] D.-X. Xue, A. J. Cairns, Y. Belmabkhout, Ł. Wojtas, Y. Liu, M. H. Alkordi, M. Eddaoudi, *J. Am. Chem. Soc.* **2013**, *135*, 7660–7667.
- [61] V. Guillermin, Ł. J. Weseliński, Y. Belmabkhout, A. J. Cairns, V. D'Elia, Ł. Wojtas, K. Adil, M. Eddaoudi, *Nat. Chem.* **2014**, *6*, 673–680.
- [62] M. J. Kalmutzki, N. Hanikel, O. M. Yaghi, *Sci. Adv.* **2018**, *4*, eaat9180.
- [63] V. Bon, V. Senkovskyy, I. Senkovska, S. Kaskel, *Chem. Commun.* **2012**, *48*, 8407–8409.
- [64] D. Alezi, A. M. P. Peedikakkal, Ł. J. Weseliński, V. Guillermin, Y. Belmabkhout, A. J. Cairns, Z. Chen, Ł. Wojtas, M. Eddaoudi, *J. Am. Chem. Soc.* **2015**, *137*, 5421–5430.
- [65] D. Feng, Z. Y. Gu, Y. P. Chen, J. Park, Z. Wei, Y. Sun, M. Bosch, S. Yuan, H. C. Zhou, *J. Am. Chem. Soc.* **2014**, *136*, 17714–17717.
- [66] S. E. Gilson, P. Li, J. E. S. Szymanowski, J. White, D. Ray, L. Gagliardi, O. K. Farha, P. C. Burns, *J. Am. Chem. Soc.* **2019**, *141*, 11842–11846.
- [67] D. Y. Du, J. S. Qin, Z. Sun, L. K. Yan, M. O'Keeffe, Z. M. Su, S. L. Li, X. H. Wang, X. L. Wang, Y. Q. Lan, *Sci. Rep.* **2013**, *3*, 2616.
- [68] L. Liu, K. Konstas, M. R. Hill, S. G. Telfer, *J. Am. Chem. Soc.* **2013**, *135*, 17731–17734.
- [69] S. Yuan, J. S. Qin, J. Li, L. Huang, L. Feng, Y. Fang, C. Lollar, J. Pang, L. Zhang, D. Sun, A. Alsalmé, T. Cagin, H. C. Zhou, *Nat. Commun.* **2018**, *9*, 808.
- [70] K. Koh, A. G. Wong-Foy, A. J. Matzger, *Angew. Chem. Int. Ed.* **2008**, *47*, 677–680; *Angew. Chem.* **2008**, *120*, 689–692.
- [71] L. Liu, S. G. Telfer, *J. Am. Chem. Soc.* **2015**, *137*, 3901–3909.
- [72] B. Tu, L. Diestel, Z. Shi, W. R. L. N. Bandara, Y. Chen, W. Lin, Y. Zhang, S. G. Telfer, Q. Li, *Angew. Chem. Int. Ed.* **2019**, *58*, 5348–5353; *Angew. Chem.* **2019**, *131*, 5402–5407.
- [73] L. K. Macreadie, R. Babarao, C. J. Setter, S. J. Lee, O. T. Qazvini, A. J. Seeber, J. Tsanaktisidis, S. G. Telfer, S. R. Batten, M. R. Hill, *Angew. Chem. Int. Ed.* **2020**, *59*, 6090–6098; *Angew. Chem.* **2020**, *132*, 6146–6154.
- [74] L. Feng, K. Y. Wang, G. S. Day, H. C. Zhou, *Chem. Soc. Rev.* **2019**, *48*, 4823–4853.
- [75] T. Y. Zhou, B. Auer, S. J. Lee, S. G. Telfer, *J. Am. Chem. Soc.* **2019**, *141*, 1577–1582.
- [76] B. Tu, Q. Pang, E. Ning, W. Yan, Y. Qi, D. Wu, Q. Li, *J. Am. Chem. Soc.* **2015**, *137*, 13456–13459.
- [77] K. Seki, S. Takamizawa, W. Mori, *Chem. Lett.* **2001**, *30*, 332–333.
- [78] F. A. A. Paz, J. Klinowski, S. M. F. Vilela, J. P. C. Tomé, J. A. S. Cavaleiro, J. Rocha, *Chem. Soc. Rev.* **2012**, *41*, 1088–1110.
- [79] A. Helal, Z. H. Yamani, K. E. Cordova, O. M. Yaghi, *Natl. Sci. Rev.* **2017**, *4*, 296–298.
- [80] J. Jiang, O. M. Yaghi, *Chem. Rev.* **2015**, *115*, 6966–6997.
- [81] L. J. Wang, H. Deng, H. Furukawa, F. Gándara, K. E. Cordova, D. Peri, O. M. Yaghi, *Inorg. Chem.* **2014**, *53*, 5881–5883.
- [82] Y. B. Zhang, H. Furukawa, N. Ko, W. Nie, H. J. Park, S. Okajima, K. E. Cordova, H. Deng, J. Kim, O. M. Yaghi, *J. Am. Chem. Soc.* **2015**, *137*, 2641–2650.
- [83] Z. Dong, Y. Sun, J. Chu, X. Zhang, H. Deng, *J. Am. Chem. Soc.* **2017**, *139*, 14209–14216.
- [84] Q. Liu, Y. Song, Y. Ma, Y. Zhou, H. Cong, C. Wang, J. Wu, G. Hu, M. O'Keeffe, H. Deng, *J. Am. Chem. Soc.* **2019**, *141*, 488–496.
- [85] I. Abánades Lázaro, C. J. R. Wells, R. S. Forgan, *Angew. Chem. Int. Ed.* **2020**, *59*, 5211–5217; *Angew. Chem.* **2020**, *132*, 5249–5255.
- [86] Z. Ji, H. Wang, S. Canossa, S. Wuttke, O. M. Yaghi, *Adv. Funct. Mater.* **2020**, *30*, 2000238.
- [87] W. Xu, B. Tu, Q. Liu, Y. Shu, C. C. Liang, C. S. Diercks, O. M. Yaghi, Y. B. Zhang, H. Deng, Q. Li, *Nat. Rev. Mater.* **2020**, *5*, 764–779.
- [88] R. Kitaura, K. Fujimoto, S. Noro, M. Kondo, S. Kitagawa, *Angew. Chem. Int. Ed.* **2002**, *41*, 133–135; *Angew. Chem.* **2002**, *114*, 141–143.
- [89] H. Deng, C. J. Doonan, H. Furukawa, R. B. Ferreira, J. Towne, C. B. Knobler, B. Wang, O. M. Yaghi, *Science* **2010**, *327*, 846–850.
- [90] Q. Liu, H. Cong, H. Deng, *J. Am. Chem. Soc.* **2016**, *138*, 13822–13825.
- [91] A. M. Fracaroli, P. Siman, D. A. Nagib, M. Suzuki, H. Furukawa, F. D. Toste, O. M. Yaghi, *J. Am. Chem. Soc.* **2016**, *138*, 8352–8355.
- [92] C. Tan, X. Han, Z. Li, Y. Liu, Y. Cui, *J. Am. Chem. Soc.* **2018**, *140*, 16229–16236.
- [93] C. A. Trickett, K. J. Gagnon, S. Lee, F. Gándara, H. B. Bürgi, O. M. Yaghi, *Angew. Chem. Int. Ed.* **2015**, *54*, 11162–11167; *Angew. Chem.* **2015**, *127*, 11314–11319.
- [94] Y. Wang, Q. Liu, Q. Zhang, B. Peng, H. Deng, *Angew. Chem. Int. Ed.* **2018**, *57*, 7120–7125; *Angew. Chem.* **2018**, *130*, 7238–7243.
- [95] Y. B. Zhang, J. Su, H. Furukawa, Y. Yun, F. Gándara, A. Duong, X. Zou, O. M. Yaghi, *J. Am. Chem. Soc.* **2013**, *135*, 16336–16339.
- [96] Y. Liu, Y. Ma, Y. Zhao, X. Sun, F. Gándara, H. Furukawa, Z. Liu, H. Zhu, C. Zhu, K. Suenaga, et al., *Science* **2016**, *351*, 365–369.
- [97] E. Jin, M. Asada, Q. Xu, S. Dalapati, M. A. Addicoat, M. A. Brady, H. Xu, T. Nakamura, T. Heine, Q. Chen, et al., *Science* **2017**, *357*, 673–676.

- [98] T. Ma, E. A. Kapustin, S. X. Yin, L. Liang, Z. Zhou, J. Niu, L. H. Li, Y. Wang, J. Su, J. Li, et al., *Science* **2018**, *361*, 48–52.
- [99] A. M. Evans, L. R. Parent, N. C. Flanders, R. P. Bisbey, E. Vitaku, M. S. Kirschner, R. D. Schaller, L. X. Chen, N. C. Gianneschi, W. R. Dichtel, *Science* **2018**, *361*, 52–57.
- [100] Y. Liu, C. S. Diercks, Y. Ma, H. Lyu, C. Zhu, S. A. Alshimiri, S. Alshihri, O. M. Yaghi, *J. Am. Chem. Soc.* **2019**, *141*, 677–683.
- [101] C. Gropp, T. Ma, N. Hanikel, O. M. Yaghi, *Science* **2020**, *370*, eabd6406.
- [102] G. Veber, C. S. Diercks, C. Rogers, W. S. Perkins, J. Ciston, K. Lee, J. P. Llinas, A. Liebman-Peláez, C. Zhu, J. Bokor, et al., *Chem* **2020**, *6*, 1125–1133.
- [103] Y. Du, H. Yang, J. M. Whiteley, S. Wan, Y. Jin, S. H. Lee, W. Zhang, *Angew. Chem. Int. Ed.* **2016**, *55*, 1737–1741; *Angew. Chem.* **2016**, *128*, 1769–1773.
- [104] Y. Zhang, J. Duan, D. Ma, P. Li, S. Li, H. Li, J. Zhou, X. Ma, X. Feng, B. Wang, *Angew. Chem. Int. Ed.* **2017**, *56*, 16313–16317; *Angew. Chem.* **2017**, *129*, 16531–16535.
- [105] F. J. Uribe-Romo, J. R. Hunt, H. Furukawa, C. Klöck, M. O’Keeffe, O. M. Yaghi, *J. Am. Chem. Soc.* **2009**, *131*, 4570–4571.
- [106] F. J. Uribe-Romo, C. J. Doonan, H. Furukawa, K. Oisaki, O. M. Yaghi, *J. Am. Chem. Soc.* **2011**, *133*, 11478–11481.
- [107] A. Nagai, X. Chen, X. Feng, X. Ding, Z. Guo, D. Jiang, *Angew. Chem. Int. Ed.* **2013**, *52*, 3770–3774; *Angew. Chem. Int. Ed.* **2013**, *125*, 3858–3862.
- [108] C. R. Deblase, K. E. Silberstein, T. T. Truong, H. D. Abruña, W. R. Dichtel, *J. Am. Chem. Soc.* **2013**, *135*, 16821–16824.
- [109] J. Guo, Y. Xu, S. Jin, L. Chen, T. Kajji, Y. Honsho, M. A. Addicoat, J. Kim, A. Saeki, H. Ihee, et al., *Nat. Commun.* **2013**, *4*, 2736.
- [110] P. J. Waller, S. J. Lyle, T. M. Osborn Popp, C. S. Diercks, J. A. Reimer, O. M. Yaghi, *J. Am. Chem. Soc.* **2016**, *138*, 15519–15522.
- [111] H. Liu, J. Chu, Z. Yin, X. Cai, L. Zhuang, H. Deng, *Chem* **2018**, *4*, 1696–1709.
- [112] P. J. Waller, Y. S. Alfaraj, C. S. Diercks, N. N. Jarewattananon, O. M. Yaghi, *J. Am. Chem. Soc.* **2018**, *140*, 9099–9103.
- [113] K. T. Jackson, T. E. Reich, H. M. El-Kaderi, *Chem. Commun.* **2012**, *48*, 8823–8825.
- [114] Q. Fang, Z. Zhuang, S. Gu, R. B. Kaspar, J. Zheng, J. Wang, S. Qiu, Y. Yan, *Nat. Commun.* **2014**, *5*, 4503.
- [115] H. Lyu, C. S. Diercks, C. Zhu, O. M. Yaghi, *J. Am. Chem. Soc.* **2019**, *141*, 6848–6852.
- [116] T. Ma, E. A. Kapustin, S. X. Yin, L. Liang, Z. Zhou, J. Niu, L. H. Li, Y. Wang, J. Su, J. Li, X. Wang, W. D. Wang, W. Wang, J. Sun, O. M. Yaghi, *Science* **2018**, *361*, 48–52.
- [117] Q. Zhu, X. Wang, R. Clowes, P. Cui, L. Chen, M. A. Little, A. I. Cooper, *J. Am. Chem. Soc.* **2020**, *142*, 16842–16848.
- [118] G. Veber, C. S. Diercks, C. Rogers, W. S. Perkins, J. Ciston, K. Lee, J. P. Llinas, A. Liebman-Peláez, C. Zhu, J. Bokor, et al., *Chem* **2020**, *6*, 1125–1133.
- [119] Y. Liu, Y. Ma, J. Yang, C. S. Diercks, N. Tamura, F. Jin, O. M. Yaghi, *J. Am. Chem. Soc.* **2018**, *140*, 16015–16019.
- [120] Y. Liu, C. S. Diercks, Y. Ma, H. Lyu, C. Zhu, S. A. Alshimiri, S. Alshihri, O. M. Yaghi, *J. Am. Chem. Soc.* **2019**, *141*, 677–683.
- [121] Y. Tian, C. Cai, Y. Ji, X. You, S. Peng, G. Lee, *Angew. Chem. Int. Ed.* **2002**, *41*, 1384–1386; *Angew. Chem.* **2002**, *114*, 1442–1444.
- [122] X. Huang, J. Zhang, X. Chen, *Chinese Sci. Bull.* **2003**, *48*, 1531–1534.
- [123] K. S. Park, Z. Ni, A. P. Côté, J. Y. Choi, R. Huang, F. J. Uribe-Romo, H. K. Chae, M. O’Keeffe, O. M. Yaghi, *Proc. Natl. Acad. Sci. USA* **2006**, *103*, 10186–10191.
- [124] X. C. Huang, Y. Y. Lin, J. P. Zhang, X. M. Chen, *Angew. Chem. Int. Ed.* **2006**, *45*, 1557–1559.
- [125] H. Hayashi, A. P. Côté, H. Furukawa, M. O’Keeffe, O. M. Yaghi, *Nat. Mater.* **2007**, *6*, 501–506.
- [126] Y. Q. Tian, Y. M. Zhao, Z. X. Chen, G. N. Zhang, L. H. Weng, D. Y. Zhao, *Chem. Eur. J.* **2007**, *13*, 4146–4154.
- [127] R. Banerjee, A. Phan, B. Wang, C. Knobler, H. Furukawa, M. O’Keeffe, O. M. Yaghi, *Science* **2008**, *319*, 939–943.
- [128] A. Phan, C. J. Doonan, F. J. Uribe-Romo, C. B. Knobler, M. O’Keeffe, O. M. Yaghi, *Acc. Chem. Res.* **2010**, *43*, 58–67.
- [129] J. Yang, Y. B. Zhang, Q. Liu, C. A. Trickett, E. Gutiérrez-Puebla, M. Á. Monge, H. Cong, A. Aldossary, H. Deng, O. M. Yaghi, *J. Am. Chem. Soc.* **2017**, *139*, 6448–6455.
- [130] S. M. Auerbach, K. A. Carrado, P. K. Dutta, *Handbook of Zeolite Science and Technology*, CRC Press, San Diego, **2003**.
- [131] A. Phan, C. J. Doonan, F. J. Uribe-Romo, C. B. Knobler, M. O’Keeffe, O. M. Yaghi, *Acc. Chem. Res.* **2010**, *43*, 58–67.
- [132] J. P. Zhang, Y. B. Zhang, J. Bin Lin, X. M. Chen, *Chem. Rev.* **2012**, *112*, 1001–1033.
- [133] M. Eddaoudi, D. F. Sava, J. F. Eubank, K. Adil, V. Guillerm, *Chem. Soc. Rev.* **2015**, *44*, 228–249.
- [134] X. C. Huang, Y. Y. Lin, J. P. Zhang, X. M. Chen, *Angew. Chem. Int. Ed.* **2006**, *45*, 1557–1559; *Angew. Chem.* **2006**, *118*, 1587–1589.
- [135] L. B. McCusker, D. H. Olson, C. Baerlocher, *Atlas of Zeolite Framework Types*, Elsevier, Amsterdam, **2007**.
- [136] B. Wang, A. P. Côté, H. Furukawa, M. O’Keeffe, O. M. Yaghi, *Nature* **2008**, *453*, 207–211.
- [137] N. T. T. Nguyen, H. Furukawa, F. Gándara, H. T. Nguyen, K. E. Cordova, O. M. Yaghi, *Angew. Chem. Int. Ed.* **2014**, *53*, 10645–10648; *Angew. Chem.* **2014**, *126*, 10821–10824.
- [138] C. Wiktor, M. Meledina, S. Turner, O. I. Lebedev, R. A. Fischer, *J. Mater. Chem. A* **2017**, *5*, 14969–14989.
- [139] P. Cubillas, M. W. Anderson, M. P. Attfield, *Chem. Eur. J.* **2012**, *18*, 15406–15415.
- [140] P. Hirschle, T. Preiß, F. Auras, A. Pick, J. Völkner, D. Valdepérez, G. Witte, W. J. Parak, J. O. Rädler, S. Wuttke, *CrystEngComm* **2016**, *18*, 4359–4368.
- [141] R. A. Maia, L. S. D. A. Carneiro, J. M. C. Cifuentes, C. D. Buarque, P. M. Esteves, A. M. Percebon, *J. Appl. Crystallogr.* **2020**, *53*, 1376–1386.
- [142] F. Gándara, T. D. Bennett, *IUCrJ* **2014**, *1*, 563–570.
- [143] P. A. Julien, K. Užarević, A. D. Katsenis, S. A. J. Kimber, T. Wang, O. K. Farha, Y. Zhang, J. Casaban, L. S. Germann, M. Etter, et al., *J. Am. Chem. Soc.* **2016**, *138*, 2929–2932.
- [144] Z. Huang, E. S. Grape, J. Li, A. K. Inge, X. Zou, *Coord. Chem. Rev.* **2021**, *427*, 213583.
- [145] N. Rosenbach, H. Jovic, A. Ghoufi, F. Salles, G. Maurin, S. Bourrelly, P. L. Llewellyn, T. Devic, C. Serre, G. Férey, *Angew. Chem. Int. Ed.* **2008**, *47*, 6611–6615; *Angew. Chem.* **2008**, *120*, 6713–6717.
- [146] C. M. Brown, Y. U. N. Liu, D. A. N. A. Neumann, *Pramana* **2008**, *71*, 755–760.
- [147] F. Salles, H. Jovic, A. Ghoufi, P. L. Llewellyn, C. Serre, S. Bourrelly, G. Férey, G. Maurin, *Angew. Chem. Int. Ed.* **2009**, *48*, 8335–8339; *Angew. Chem.* **2009**, *121*, 8485–8489.
- [148] J. X. Jiang, F. Su, A. Trewin, C. D. Wood, H. Niu, J. T. A. Jones, Y. Z. Khimyak, A. I. Cooper, *J. Am. Chem. Soc.* **2008**, *130*, 7710–7720.
- [149] L. Liu, Z. Chen, J. Wang, D. Zhang, Y. Zhu, S. Ling, K. W. Huang, Y. Belmabkhout, K. Adil, Y. Zhang, et al., *Nat. Chem.* **2019**, *11*, 622–628.
- [150] F. I. Pambudi, M. W. Anderson, M. P. Attfield, *Chem. Sci.* **2019**, *10*, 9571–9575.
- [151] M. A. Van Der Veen, T. Verbiest, D. E. De Vos, *Microporous Mesoporous Mater.* **2013**, *166*, 102–108.
- [152] X. Kang, K. Lyu, L. Li, J. Li, L. Kimberley, B. Wang, L. Liu, Y. Cheng, M. D. Frogley, S. Rudić, et al., *Nat. Commun.* **2019**, *10*, 4466.
- [153] W. Schrimpf, J. Jiang, Z. Ji, P. Hirschle, D. C. Lamb, O. M. Yaghi, S. Wuttke, *Nat. Commun.* **2018**, *9*, 1647.

- [154] Z. Ji, T. Li, O. M. Yaghi, *Science* **2020**, *369*, 674–680.
- [155] C. Castillo-Blas, J. M. Moreno, I. Romero-Muñiz, A. E. Platero-Prats, *Nanoscale* **2020**, *12*, 15577–15587.
- [156] S. Li, O. Lafon, W. Wang, Q. Wang, X. Wang, Y. Li, J. Xu, F. Deng, *Adv. Mater.* **2020**, *32*, 2002879.
- [157] X. Zhang, Z. Chen, X. Liu, S. L. Hanna, X. Wang, R. Taheri-Ledari, A. Maleki, P. Li, O. K. Farha, *Chem. Soc. Rev.* **2020**, *49*, 7406–7427.
- [158] C. S. Tsao, M. S. Yu, T. Y. Chung, H. C. Wu, C. Y. Wang, K. Sen Chang, H. L. Chen, *J. Am. Chem. Soc.* **2007**, *129*, 15997–16004.
- [159] I. Beurroies, M. Boulhout, P. L. Llewellyn, B. Kuchta, G. Férey, C. Serre, R. Denoyel, *Angew. Chem. Int. Ed.* **2010**, *49*, 7526–7529; *Angew. Chem.* **2010**, *122*, 7688–7691.
- [160] Q. Song, S. K. Nataraj, M. V. Roussanova, J. C. Tan, D. J. Hughes, W. Li, P. Bourgoïn, M. A. Alam, A. K. Cheetham, S. A. Al-Muhtaseb, et al., *Energy Environ. Sci.* **2012**, *5*, 8359–8369.
- [161] H. Lyu, Z. Ji, S. Wuttke, O. M. Yaghi, *Chem* **2020**, *6*, 2219–2241.
- [162] O. M. Yaghi, G. Li, H. Li, *Nature* **1995**, *378*, 703–706.
- [163] H. Li, M. Eddaoudi, M. O’Keeffe, O. M. Yaghi, *Nature* **1999**, *402*, 276–279.
- [164] L. M. Rodriguez-Albelo, A. R. Ruiz-Salvador, A. Sampieri, D. W. Lewis, A. Gómez, B. Nohra, P. Mialane, J. Marrot, F. Sécheresse, C. Mellot-Draznieks, et al., *J. Am. Chem. Soc.* **2009**, *131*, 16078–16087.
- [165] M. A. Addicoat, D. E. Coupry, T. Heine, *J. Phys. Chem. A* **2014**, *118*, 9607–9614.
- [166] V. Bernales, M. A. Ortuño, D. G. Truhlar, C. J. Cramer, L. Gagliardi, *ACS Cent. Sci.* **2018**, *4*, 5–19.
- [167] T. Düren, Y. S. Bae, R. Q. Snurr, *Chem. Soc. Rev.* **2009**, *38*, 1237–1247.
- [168] N. A. Ramsahye, G. Maurin, S. Bourrelly, P. L. Llewellyn, T. Loiseau, C. Serre, G. Férey, *Chem. Commun.* **2007**, 3261–3263.
- [169] S. L. Mayo, B. D. Olafson, W. A. Goddard, *J. Phys. Chem.* **1990**, *94*, 8897–8909.
- [170] A. K. Rappe, C. J. Casewit, K. S. Colwell, W. A. Goddard, W. M. Skiff, *J. Am. Chem. Soc.* **1992**, *114*, 10024–10035.
- [171] W. L. Jorgensen, J. Tirado-Rives, *J. Am. Chem. Soc.* **1988**, *110*, 1657–1666.
- [172] D. Dubbeldam, K. S. Walton, D. E. Ellis, R. Q. Snurr, *Angew. Chem. Int. Ed.* **2007**, *46*, 4496–4499; *Angew. Chem.* **2007**, *119*, 4580–4583.
- [173] S. Bureekaew, S. Amirjalayer, M. Tafipolsky, C. Spickermann, T. K. Roy, R. Schmid, *Phys. Status Solidi B* **2013**, *250*, 1128–1141.
- [174] J. K. Bristow, D. Tiana, A. Walsh, *J. Chem. Theory Comput.* **2014**, *10*, 4644–4652.
- [175] J. K. Bristow, J. M. Skelton, K. L. Svane, A. Walsh, J. D. Gale, *Phys. Chem. Chem. Phys.* **2016**, *18*, 29316–29329.
- [176] D. E. Coupry, M. A. Addicoat, T. Heine, *J. Chem. Theory Comput.* **2016**, *12*, 5215–5225.
- [177] X. P. Wu, L. Gagliardi, D. G. Truhlar, *J. Chem. Theory Comput.* **2019**, *15*, 4208–4217.
- [178] M. Zheng, Y. Liu, C. Wang, S. Liu, W. Lin, *Chem. Sci.* **2012**, *3*, 2623–2627.
- [179] D. Dubbeldam, K. S. Walton, D. E. Ellis, R. Q. Snurr, *Angew. Chem. Int. Ed.* **2007**, *46*, 4496–4499.
- [180] C. E. Wilmer, M. Leaf, C. Y. Lee, O. K. Farha, B. G. Hauser, J. T. Hupp, R. Q. Snurr, *Nat. Chem.* **2012**, *4*, 83–89.
- [181] S. Bureekaew, S. Amirjalayer, M. Tafipolsky, C. Spickermann, T. K. Roy, R. Schmid, *Phys. Status Solidi B* **2013**, *250*, 1128–1141.
- [182] Y. G. Chung, J. Camp, M. Haranczyk, B. J. Sikora, W. Bury, V. Krungleviciute, T. Yildirim, O. K. Farha, D. S. Sholl, R. Q. Snurr, *Chem. Mater.* **2014**, *26*, 6185–6192.
- [183] P. Z. Moghadam, A. Li, S. B. Wiggin, A. Tao, A. G. P. Maloney, P. A. Wood, S. C. Ward, D. Fairen-Jimenez, *Chem. Mater.* **2017**, *29*, 2618–2625.
- [184] M. Tafipolsky, S. Amirjalayer, R. Schmid, *J. Comput. Chem.* **2007**, *28*, 1169–1176.
- [185] A. I. Skoulidas, D. S. Sholl, *J. Phys. Chem. B* **2005**, *109*, 15760–15768.
- [186] J. A. Greathouse, M. D. Allendorf, *J. Am. Chem. Soc.* **2006**, *128*, 10678–10679.
- [187] Y. G. Chung, J. Camp, M. Haranczyk, B. J. Sikora, W. Bury, V. Krungleviciute, T. Yildirim, O. K. Farha, D. S. Sholl, R. Q. Snurr, *Chem. Mater.* **2014**, *26*, 6185–6192.
- [188] M. Tong, Y. Lan, Q. Yang, C. Zhong, *Chem. Eng. Sci.* **2017**, *168*, 456–464.
- [189] C. E. Wilmer, M. Leaf, C. Y. Lee, O. K. Farha, B. G. Hauser, J. T. Hupp, R. Q. Snurr, *Nat. Chem.* **2012**, *4*, 83–89.
- [190] R. Mercado, R. S. Fu, A. V. Yakutovich, L. Talirz, M. Haranczyk, B. Smit, *Chem. Mater.* **2018**, *30*, 5069–5086.
- [191] A. Ahmed, Y. Liu, J. Purewal, L. D. Tran, A. G. Wong-Foy, M. Veenstra, A. J. Matzger, D. J. Siegel, *Energy Environ. Sci.* **2017**, *10*, 2459–2471.
- [192] P. G. Boyd, A. Chidambaram, E. García-Díez, C. P. Ireland, T. D. Daff, R. Bounds, A. Gładysiak, P. Schouwink, S. M. Moosavi, M. M. Maroto-Valer, et al., *Nature* **2019**, *576*, 253–256.
- [193] B. F. Hoskins, R. Robson, *J. Am. Chem. Soc.* **1990**, *112*, 1546–1554.
- [194] Y. H. Kiang, G. B. Gardner, S. Lee, Z. Xu, E. B. Lobkovsky, *J. Am. Chem. Soc.* **1999**, *121*, 8204–8215.
- [195] Y. H. Kiang, G. B. Gardner, S. Lee, Z. Xu, *J. Am. Chem. Soc.* **2000**, *122*, 6871–6883.
- [196] Z. Wang, S. M. Cohen, *J. Am. Chem. Soc.* **2007**, *129*, 12368–12369.
- [197] S. Das, H. Kim, O. Kim, *J. Am. Chem. Soc.* **2009**, *131*, 3814–3815.
- [198] B. J. Burnett, P. M. Barron, C. Hu, W. Choe, *J. Am. Chem. Soc.* **2011**, *133*, 9984–9987.
- [199] S. Pullen, H. Fei, A. Orthaber, S. M. Cohen, S. Ott, *J. Am. Chem. Soc.* **2013**, *135*, 16997–17003.
- [200] L. Garzón-Tovar, S. Rodríguez-Hermida, I. Imaz, D. Maspocho, *J. Am. Chem. Soc.* **2017**, *139*, 897–903.
- [201] J. Albalad, H. Xu, F. Gándara, M. Haouas, C. Martineau-Corcós, R. Mas-Ballesté, S. A. Barnett, J. Juanhuix, I. Imaz, D. Maspocho, *J. Am. Chem. Soc.* **2018**, *140*, 2028–2031.
- [202] J. S. Qin, S. Yuan, L. Zhang, B. Li, D. Y. Du, N. Huang, W. Guan, H. F. Drake, J. Pang, Y. Q. Lan, et al., *J. Am. Chem. Soc.* **2019**, *141*, 2054–2060.
- [203] K. K. Tanabe, Z. Wang, S. M. Cohen, *J. Am. Chem. Soc.* **2008**, *130*, 8508–8517.
- [204] J. G. Nguyen, S. M. Cohen, *J. Am. Chem. Soc.* **2010**, *132*, 4560–4561.
- [205] D. R. Du Bois, A. J. Matzger, *J. Am. Chem. Soc.* **2021**, *143*, 671–674.
- [206] Z. Wang, S. M. Cohen, *Angew. Chem. Int. Ed.* **2008**, *47*, 4699–4702; *Angew. Chem.* **2008**, *120*, 4777–4780.
- [207] M. Kalaj, S. M. Cohen, *Angew. Chem.* **2020**, *132*, 14088–14093.
- [208] M. J. Ingleson, J. Perez Barrio, J. B. Guilbaud, Y. Z. Khimyak, M. J. Rosseinsky, *Chem. Commun.* **2008**, 2680–2682.
- [209] F. G. Xi, H. Liu, N. N. Yang, E. Q. Gao, *Inorg. Chem.* **2016**, *55*, 4701–4703.
- [210] A. D. Burrows, C. G. Frost, M. F. Mahon, C. Richardson, *Angew. Chem.* **2008**, *120*, 8610–8614.
- [211] W. Morris, C. J. Doonan, H. Furukawa, R. Banerjee, O. M. Yaghi, *J. Am. Chem. Soc.* **2008**, *130*, 12626–12627.
- [212] K. K. Tanabe, C. A. Allen, S. M. Cohen, *Angew. Chem.* **2010**, *49*, 9730–9733.

- [213] R. K. Deshpande, J. L. Minnaar, S. G. Telfer, *Angew. Chem.* **2010**, *122*, 4702–4706.
- [214] T. Gadzikwa, G. Lu, C. L. Stern, S. R. Wilson, J. T. Hupp, S. T. Nguyen, *Chem. Commun.* **2008**, 5493–5495.
- [215] M. Lalonde, W. Bury, O. Karagiari, Z. Brown, J. T. Hupp, O. K. Farha, *J. Mater. Chem. A* **2013**, *1*, 5453–5468.
- [216] C. K. Brozek, M. Dincă, *Chem. Soc. Rev.* **2014**, *43*, 5456–5467.
- [217] S. J. Garibay, Z. Wang, K. K. Tanabe, S. M. Cohen, *Inorg. Chem.* **2009**, *48*, 7341–7349.
- [218] M. Kim, J. F. Cahill, H. Fei, K. A. Prather, S. M. Cohen, *J. Am. Chem. Soc.* **2012**, *134*, 18082–18088.
- [219] M. S. Denny, L. R. Parent, J. P. Patterson, S. K. Meena, H. Pham, P. Abellan, Q. M. Ramasse, F. Paesani, N. C. Gianneschi, S. M. Cohen, *J. Am. Chem. Soc.* **2018**, *140*, 1348–1357.
- [220] C. Liu, T. Y. Luo, E. S. Feura, C. Zhang, N. L. Rosi, *J. Am. Chem. Soc.* **2015**, *137*, 10508–10511.
- [221] C. Liu, C. Zeng, T. Y. Luo, A. D. Merg, R. Jin, N. L. Rosi, *J. Am. Chem. Soc.* **2016**, *138*, 12045–12048.
- [222] M. Kim, J. F. Cahill, Y. Su, K. A. Prather, S. M. Cohen, *Chem. Sci.* **2012**, *3*, 126–130.
- [223] R. J. Marshall, S. L. Griffin, C. Wilson, R. S. Forgan, *J. Am. Chem. Soc.* **2015**, *137*, 9527–9530.
- [224] Z. Wang, S. M. Cohen, *J. Am. Chem. Soc.* **2009**, *131*, 16675–16677.
- [225] S. J. Garibay, S. M. Cohen, *Chem. Commun.* **2010**, *46*, 7700–7702.
- [226] T. Ishiwata, Y. Furukawa, K. Sugikawa, K. Kokado, K. Sada, *J. Am. Chem. Soc.* **2013**, *135*, 5427–5432.
- [227] T. Ishiwata, K. Kokado, K. Sada, *Angew. Chem. Int. Ed.* **2017**, *56*, 2608–2612; *Angew. Chem.* **2017**, *129*, 2652–2656.
- [228] L. Feng, X. L. Lv, T. H. Yan, H. C. Zhou, *J. Am. Chem. Soc.* **2019**, *141*, 10342–10349.
- [229] S. Wang, C. M. McGuirk, A. d'Aquino, J. A. Mason, C. A. Mirkin, *Adv. Mater.* **2018**, *30*, 1800202.
- [230] E. Ploetz, H. Engelke, U. Lächelt, S. Wuttke, *Adv. Funct. Mater.* **2020**, *30*, 1909062.
- [231] X. Cai, Z. Xie, D. Li, M. Kassymova, S. Q. Zang, H. L. Jiang, *Coord. Chem. Rev.* **2020**, *417*, 213366.
- [232] E. A. Flügel, A. Ranft, F. Haase, B. V. Lotsch, *J. Mater. Chem.* **2012**, *22*, 10119–10133.
- [233] V. K. LaMer, R. H. Dinegar, *J. Am. Chem. Soc.* **1950**, *72*, 4847–4854.
- [234] J. Cravillon, R. Nayuk, S. Springer, A. Feldhoff, K. Huber, M. Wiebcke, *Chem. Mater.* **2011**, *23*, 2130–2141.
- [235] M. Oh, C. A. Mirkin, *Nature* **2005**, *438*, 651–654.
- [236] Z. Ni, R. I. Masel, *J. Am. Chem. Soc.* **2006**, *128*, 12394–12395.
- [237] E. Haque, N. A. Khan, C. M. Kim, S. H. Jung, *Cryst. Growth Des.* **2011**, *11*, 4413–4421.
- [238] A. Laybourn, J. Katrib, R. S. Ferrari-John, C. G. Morris, S. Yang, O. Udoudo, T. L. Easun, C. Dodds, N. R. Champness, S. W. Kingman, et al., *J. Mater. Chem. A* **2017**, *5*, 7333–7338.
- [239] W. J. Son, J. Kim, J. Kim, W. S. Ahn, *Chem. Commun.* **2008**, 6336–6338.
- [240] E. Haque, N. A. Khan, H. J. Park, S. H. Jung, *Chem. Eur. J.* **2010**, *16*, 1046–1052.
- [241] K. J. Kim, Y. J. Li, P. B. Kreider, C. H. Chang, N. Wannemacher, P. K. Thallapally, H. G. Ahn, *Chem. Commun.* **2013**, 49, 11518–11520.
- [242] S. Watanabe, S. Ohsaki, T. Hanafusa, K. Takada, H. Tanaka, K. Mae, M. T. Miyahara, *Chem. Eng. J.* **2017**, *313*, 724–733.
- [243] D. Tanaka, A. Henke, K. Albrecht, M. Moeller, K. Nakagawa, S. Kitagawa, J. Groll, *Nat. Chem.* **2010**, *2*, 410–416.
- [244] M. Pang, A. J. Cairns, Y. Liu, Y. Belmabkhout, H. C. Zeng, M. Eddaoudi, *J. Am. Chem. Soc.* **2013**, *135*, 10234–10237.
- [245] M. M. Modena, B. Rühle, T. P. Burg, S. Wuttke, *Adv. Mater.* **2019**, *31*, 1970226.
- [246] P. Hirschle, T. Preiß, F. Auras, A. Pick, J. Völkner, D. Valdepérez, G. Witte, W. J. Parak, J. O. Rädler, S. Wuttke, *CrystEngComm* **2016**, *18*, 4359–4368.
- [247] B. J. Smith, L. R. Parent, A. C. Overholt, P. A. Beaucage, R. P. Bisbey, A. D. Chavez, N. Hwang, C. Park, A. M. Evans, N. C. Gianneschi, et al., *ACS Cent. Sci.* **2017**, *3*, 58–65.
- [248] S. Wang, W. Morris, Y. Liu, C. M. McGuirk, Y. Zhou, J. T. Hupp, O. K. Farha, C. A. Mirkin, *Angew. Chem. Int. Ed.* **2015**, *54*, 14738–14742; *Angew. Chem.* **2015**, *127*, 14951–14955.
- [249] W. Morris, W. E. Briley, E. Auyeung, M. D. Cabezas, C. A. Mirkin, *J. Am. Chem. Soc.* **2014**, *136*, 7261–7264.
- [250] A. Zimpel, T. Preiß, R. Röder, H. Engelke, M. Ingris, M. Peller, J. O. Rädler, E. Wagner, T. Bein, U. Lächelt, et al., *Chem. Mater.* **2016**, *28*, 3318–3326.
- [251] Y. H. Shih, S. H. Lo, N. S. Yang, B. Singco, Y. J. Cheng, C. Y. Wu, I. H. Chang, H. Y. Huang, C. H. Lin, *ChemPlusChem* **2012**, *77*, 982–986.
- [252] S. Wang, S. S. Park, C. T. Buru, H. Lin, P. C. Chen, E. W. Roth, O. K. Farha, C. A. Mirkin, *Nat. Commun.* **2020**, *11*, 2495.
- [253] C. Avci, Y. Liu, J. A. Pariente, A. Blanco, C. Lopez, I. Imaz, D. Maspocho, *Small* **2019**, *15*, 1902520.
- [254] C. Avci, I. Imaz, A. Carné-Sánchez, J. A. Pariente, N. Tasios, J. Pérez-Carvajal, M. I. Alonso, A. Blanco, M. Dijkstra, C. López, et al., *Nat. Chem.* **2018**, *10*, 78–84.
- [255] M. D. Allendorf, R. Dong, X. Feng, S. Kaskel, D. Matoga, V. Stavila, *Chem. Rev.* **2020**, *120*, 8581–8640.
- [256] P. Falcaro, K. Okada, T. Hara, K. Iikigaki, Y. Tokudome, A. W. Thornton, A. J. Hill, T. Williams, C. Doonan, M. Takahashi, *Nat. Mater.* **2017**, *16*, 342–348.
- [257] J. Hwang, A. Ejsmont, R. Freund, J. Goscińska, B. V. K. J. Schmidt, S. Wuttke, *Chem. Soc. Rev.* **2020**, *49*, 3348–3422.
- [258] S. Wuttke, D. D. Medina, J. M. Rotter, S. Begum, T. Stassin, R. Ameloot, M. Oschatz, M. Tsotsalas, *Adv. Funct. Mater.* **2018**, *28*, 1801545.
- [259] Y. Peng, Y. Li, Y. Ban, H. Jin, W. Jiao, X. Liu, W. Yang, *Science* **2014**, *346*, 1356–1359.
- [260] H. Wang, Z. Zeng, P. Xu, L. Li, G. Zeng, R. Xiao, Z. Tang, D. Huang, L. Tang, C. Lai, et al., *Chem. Soc. Rev.* **2019**, *48*, 488–516.
- [261] A. M. Evans, N. P. Bradshaw, B. Litchfield, M. J. Strauss, B. Seckman, M. R. Ryder, I. Castano, C. Gilmore, N. C. Gianneschi, C. R. Mulzer, et al., *Adv. Mater.* **2020**, *32*, 2004205.
- [262] D. W. Burke, C. Sun, I. Castano, N. C. Flanders, A. M. Evans, E. Vitaku, D. C. McLeod, R. H. Lambeth, L. X. Chen, N. C. Gianneschi, et al., *Angew. Chem. Int. Ed.* **2020**, *59*, 5165–5171; *Angew. Chem.* **2020**, *132*, 5203–5209.
- [263] E. Biemmi, C. Scherb, T. Bein, *J. Am. Chem. Soc.* **2007**, *129*, 8054–8055.
- [264] F. M. Hinterholzinger, A. Ranft, J. M. Feckl, B. Rühle, T. Bein, B. V. Lotsch, *J. Mater. Chem.* **2012**, *22*, 10356–10362.
- [265] O. Shekhah, H. Wang, S. Kowarik, F. Schreiber, M. Paulus, M. Tolan, C. Sternemann, F. Evers, D. Zacher, R. A. Fischer, C. Wöll, *J. Am. Chem. Soc.* **2007**, *129*, 15118–15119.
- [266] I. Stassen, M. Styles, G. Greci, H. Van Gorp, W. Vanderlinden, S. De Feyter, P. Falcaro, D. De Vos, P. Vereecken, R. Ameloot, *Nat. Mater.* **2016**, *15*, 304–310.
- [267] D. D. Medina, V. Werner, F. Auras, R. Tautz, M. Dogru, J. Schuster, S. Linke, M. Döblinger, J. Feldmann, P. Knochel, et al., *ACS Nano* **2014**, *8*, 4042–4052.
- [268] J. W. Colson, A. R. Woll, A. Mukherjee, M. P. Levendorf, E. L. Spitler, V. B. Shields, M. G. Spencer, J. Park, W. R. Dichtel, *Science* **2011**, *332*, 228–231.
- [269] R. Haldar, C. Wöll, *Nano Res.* **2021**, *14*, 355–368.
- [270] H. Bux, F. Liang, Y. Li, J. Cravillon, M. Wiebcke, J. Caro, *J. Am. Chem. Soc.* **2009**, *131*, 16000–16001.
- [271] D. Sheberla, L. Sun, M. A. Blood-forsythe, S. Er, C. R. Wade, C. K. Brozek, *J. Am. Chem. Soc.* **2014**, *136*, 8859–8862.

- [272] K. Liu, H. Qi, R. Dong, R. Shivhare, M. Addicoat, T. Zhang, H. Sahabudeen, T. Heine, S. Mannsfeld, U. Kaiser, Z. Zheng, et al., *Nat. Chem.* **2019**, *11*, 994–1000.
- [273] D. D. Medina, J. M. Rotter, Y. Hu, M. Dogru, V. Werner, F. Auras, J. T. Markiewicz, P. Knochel, T. Bein, *J. Am. Chem. Soc.* **2015**, *137*, 1016–1019.
- [274] S. Kandambeth, B. P. Biswal, H. D. Chaudhari, K. C. Rout, S. Kunjattu, H. S. Mitra, S. Karak, A. Das, R. Mukherjee, U. K. Kharul, et al., *Adv. Mater.* **2017**, *29*, 1603945.
- [275] E. Virmani, J. M. Rotter, A. Mähringer, T. Von Zons, A. Godt, T. Bein, S. Wuttke, D. D. Medina, *J. Am. Chem. Soc.* **2018**, *140*, 4812–4819.
- [276] J. I. Feldblyum, C. H. McCreery, S. C. Andrews, T. Kurosawa, E. J. G. Santos, V. Duong, L. Fang, A. L. Ayzner, Z. Bao, *Chem. Commun.* **2015**, *51*, 13894–13897.
- [277] B. Zhang, X. Song, Y. Li, Y. Li, Z. Peng, L. Ye, L. Chen, *Chem. Commun.* **2020**, *56*, 3253–3256.
- [278] V. Rubio-Giménez, S. Tatay, F. Volatron, F. J. Martínez-Casado, C. Martí-Gastaldo, E. Coronado, *J. Am. Chem. Soc.* **2016**, *138*, 2576–2584.
- [279] J. Huo, L. Wang, E. Irran, H. Yu, J. Gao, D. Fan, B. Li, J. Wang, W. Ding, A. M. Amin, C. Li, L. Ma, *Angew. Chem. Int. Ed.* **2010**, *49*, 9237–9241; *Angew. Chem.* **2010**, *122*, 9423–9427.
- [280] Z. Zhang, Y. Chen, X. Xu, J. Zhang, G. Xiang, W. He, X. Wang, *Angew. Chem. Int. Ed.* **2014**, *53*, 429–433; *Angew. Chem.* **2014**, *126*, 439–443.
- [281] L. Feng, J. L. Li, G. S. Day, X. L. Lv, H. C. Zhou, *Chem* **2019**, *5*, 1265–1274.
- [282] S. Kandambeth, V. Venkatesh, D. B. Shinde, S. Kumari, A. Halder, S. Verma, R. Banerjee, *Nat. Commun.* **2015**, *6*, 6786.
- [283] K. Hirai, S. Furukawa, M. Kondo, H. Uehara, O. Sakata, S. Kitagawa, *Angew. Chem. Int. Ed.* **2011**, *50*, 8057–8061; *Angew. Chem.* **2011**, *123*, 8207–8211.
- [284] R. Ameloot, F. Vermoortele, W. Vanhove, M. B. J. Roeffaers, B. F. Sels, D. E. De Vos, *Nat. Chem.* **2011**, *3*, 382–387.
- [285] N. Yanai, S. Granick, *Angew. Chem. Int. Ed.* **2012**, *51*, 5638–5641; *Angew. Chem.* **2012**, *124*, 5736–5739.
- [286] A. Carné-Sánchez, I. Imaz, M. Cano-Sarabia, D. Maspoch, *Nat. Chem.* **2013**, *5*, 203–211.
- [287] D. Crawford, J. Casaban, R. Haydon, N. Giri, T. McNally, S. L. James, *Chem. Sci.* **2015**, *6*, 1645–1649.
- [288] S. Karak, S. Kandambeth, B. P. Biswal, H. S. Sasmal, S. Kumar, P. Pachfule, R. Banerjee, *J. Am. Chem. Soc.* **2017**, *139*, 1856–1862.
- [289] K. Shen, L. Zhang, X. Chen, L. Liu, D. Zhang, Y. Han, J. Chen, J. Long, R. Luque, Y. Li, B. Chen, *Science* **2018**, *359*, 206–210.
- [290] M. Tu, B. Xia, D. E. Kravchenko, M. L. Tietze, A. J. Cruz, I. Stassen, T. Hauffman, J. Teyssandier, S. De Feyter, Z. Wang, R. A. Fischer, et al., *Nat. Mater.* **2021**, *20*, 93–99.
- [291] M. R. Lohe, M. Rose, S. Kaskel, *Chem. Commun.* **2009**, 6056–6058.
- [292] T. Tian, J. Velazquez-Garcia, T. D. Bennett, D. Fairen-Jimenez, *J. Mater. Chem. A* **2015**, *3*, 2999–3005.
- [293] B. Bueken, N. Van Velthoven, T. Willhammar, T. Stassin, I. Stassen, D. A. Keen, G. V. Baron, J. F. M. Denayer, R. Ameloot, S. Bals, et al., *Chem. Sci.* **2017**, *8*, 3939–3948.
- [294] T. Tian, Z. Zeng, D. Vulpe, M. E. Casco, G. Divitini, P. A. Midgley, J. Silvestre-Albero, J. C. Tan, P. Z. Moghadam, D. Fairen-Jimenez, *Nat. Mater.* **2018**, *17*, 174–179.
- [295] B. M. Connolly, M. Aragonés-Anglada, J. Gandara-Loe, N. A. Danaf, D. C. Lamb, J. P. Mehta, D. Vulpe, S. Wuttke, J. Silvestre-Albero, P. Z. Moghadam, et al., *Nat. Commun.* **2019**, *10*, 2345.
- [296] S. Wang, Z. Zhang, H. Zhang, A. G. Rajan, N. Xu, Y. Yang, Y. Zeng, P. Liu, X. Zhang, Q. Mao, et al., *Matter* **2019**, *1*, 1592–1605.
- [297] M. Hu, Y. Ju, K. Liang, T. Suma, J. Cui, F. Caruso, *Adv. Funct. Mater.* **2016**, *26*, 5827–5834.
- [298] J. Lee, J. H. Kwak, W. Choe, *Nat. Commun.* **2017**, *8*, 14070.
- [299] N. Yanai, M. Sindoro, J. Yan, S. Granick, *J. Am. Chem. Soc.* **2013**, *135*, 34–37.
- [300] Y. Katayama, M. Kalaj, K. S. Barcus, S. M. Cohen, *J. Am. Chem. Soc.* **2019**, *141*, 20000–20003.
- [301] H. S. Sasmal, A. Halder, S. Kunjattu, H. K. Dey, A. Nadol, T. G. Ajithkumar, P. Ravindra Bedadur, R. Banerjee, *J. Am. Chem. Soc.* **2019**, *141*, 20371–20379.
- [302] J. Reboul, S. Furukawa, N. Horike, M. Tsotsalas, K. Hirai, H. Uehara, M. Kondo, N. Louvain, O. Sakata, S. Kitagawa, *Nat. Mater.* **2012**, *11*, 717–723.
- [303] L. Yu, J. F. Yang, X. W. D. Lou, *Angew. Chem. Int. Ed.* **2016**, *55*, 13422–13426; *Angew. Chem.* **2016**, *128*, 13620–13624.
- [304] K. Hirai, J. Reboul, N. Morone, J. E. Heuser, S. Furukawa, S. Kitagawa, *J. Am. Chem. Soc.* **2014**, *136*, 14966–14973.
- [305] J. Tan, S. Namuangruk, W. Kong, N. Kungwan, J. Guo, C. Wang, *Angew. Chem. Int. Ed.* **2016**, *55*, 13979–13984; *Angew. Chem.* **2016**, *128*, 14185–14190.
- [306] M. Li, S. Qiao, Y. Zheng, Y. H. Andaloussi, X. Li, Z. Zhang, A. Li, P. Cheng, S. Ma, Y. Chen, *J. Am. Chem. Soc.* **2020**, *142*, 6675–6681.
- [307] Y. Peng, M. Zhao, B. Chen, Z. Zhang, Y. Huang, F. Dai, Z. Lai, X. Cui, C. Tan, H. Zhang, *Adv. Mater.* **2018**, *30*, 1705454.
- [308] S. Wang, Y. Yang, P. Liu, Z. Zhang, C. Zhang, A. Chen, O. O. Ajao, B.-G. Li, P. Braunstein, W.-J. Wang, *Cell Rep. Phys. Sci.* **2020**, *1*, 100062.
- [309] H. Wang, W. Zhu, J. Li, T. Tian, Y. Lan, N. Gao, C. Wang, M. Zhang, C. F. J. Faul, G. Li, *Chem. Sci.* **2015**, *6*, 1910–1916.
- [310] W. Li, Y. Zhang, Z. Xu, Q. Meng, Z. Fan, S. Ye, G. Zhang, *Angew. Chem. Int. Ed.* **2016**, *55*, 955–959; *Angew. Chem.* **2016**, *128*, 967–971.
- [311] M. Tsotsalas, H. Maheshwari, S. Schmitt, S. Heißler, W. Feng, P. A. Levkin, *Adv. Mater. Interfaces* **2016**, *3*, 1500392.
- [312] B. M. Connolly, D. G. Madden, A. E. H. Wheatley, D. Fairen-Jimenez, *J. Am. Chem. Soc.* **2020**, *142*, 8541–8549.
- [313] X. M. Liu, L. H. Xie, Y. Wu, *Inorg. Chem. Front.* **2020**, *7*, 2840–2866.
- [314] J. Cousin-Saint-Remi, S. Van Der Perre, T. Segato, M. P. Delplanck, S. Goderis, H. Terryn, G. Baron, J. Denayer, *ACS Appl. Mater. Interfaces* **2019**, *11*, 13694–13703.
- [315] A. H. Valekar, S. G. Lee, K. H. Cho, U. H. Lee, J. S. Lee, J. W. Yoon, Y. K. Hwang, S. J. Cho, J. S. Chang, *RSC Adv.* **2017**, *7*, 55767–55777.
- [316] A. I. Spjelkavik, Aarti, S. Divekar, T. Didriksen, R. Blom, *Chem. Eur. J.* **2014**, *20*, 8973–8978.
- [317] P. Z. Moghadam, S. M. J. Rogge, A. Li, C. M. Chow, J. Wieme, N. Moharrami, M. Aragonés-Anglada, G. Conduit, D. A. Gomez-Gualdrón, V. Van Speybroeck, et al., *Matter* **2019**, *1*, 219–234.
- [318] D. A. Vazquez-Molina, G. S. Mohammad-Pour, C. Lee, M. W. Logan, X. Duan, J. K. Harper, F. J. Uribe-Romo, *J. Am. Chem. Soc.* **2016**, *138*, 9767–9770.
- [319] J. P. Mehta, T. Tian, Z. Zeng, G. Divitini, B. M. Connolly, P. A. Midgley, J. C. Tan, D. Fairen-Jimenez, A. E. H. Wheatley, *Adv. Funct. Mater.* **2018**, *28*, 1705588.
- [320] J. W. Ye, X. Zhou, Y. Wang, R. K. Huang, H. L. Zhou, X. N. Cheng, Y. Ma, J. P. Zhang, *Sci. China Mater.* **2018**, *61*, 424–428.
- [321] Y. Peng, V. Krungleviciute, I. Eryazici, J. T. Hupp, O. K. Farha, T. Yildirim, *J. Am. Chem. Soc.* **2013**, *135*, 11887–11894.
- [322] J. Gallagher, *Nat. Energy* **2018**, *3*, 86.